NASA TR R-133



# NATIONAL AERONAUTICS AND SPACE ADMINISTRATION



TECHNICAL REPORT
R-133

# A PRELIMINARY THEORETICAL STUDY OF THE EXPANSION TUBE, A NEW DEVICE FOR PRODUCING HIGH-ENTHALPY SHORT-DURATION HYPERSONIC GAS FLOWS

By ROBERT L. TRIMPI

1962

For sale by the Superintendent of Documents, U.S. Government Printing Office, Washington 25, D.C. Yearly subscription, $15; foreign, $19; single copy price varies according to size ---------- Price 40 cents

Copy 1

Code 1

Single copy only

# TECHNICAL REPORT R-133

# A PRELIMINARY THEORETICAL STUDY OF THE EXPANSION TUBE, A NEW DEVICE FOR PRODUCING HIGH-ENTHALPY SHORT-DURATION HYPERSONIC GAS FLOWS

By ROBERT L. TRIMPI

Langley Research Center
Langley Station, Hampton, Va.

# TECHNICAL REPORT R-133

# A PRELIMINARY THEORETICAL STUDY OF THE EXPANSION TUBE, A NEW DEVICE FOR PRODUCING HIGH-ENTHALPY SHORT-DURATION HYPERSONIC GAS FLOWS[1]

By Robert L. Trimpi


## SUMMARY 13106

*A preliminary theoretical study was conducted of a new technique for producing high-enthalpy gas flows. The device considered utilizes an unsteady expansion process for the purpose of total-enthalpy multiplication. Analyses were conducted for both perfect and real air in equilibrium, assuming idealized diaphragm bursts, centered expansion waves, and continuum flow. Results of the study showed the expansion tube capable of outperforming the conventional shock tunnel by a factor of approximately 2 in velocity for the same test-section ambient density and pressure. The degree of dissociation is low at all phases of the thermodynamic cycle in the expansion tube; thus the test-section air has a good possibility of being in equilibrium. Maximum pressures involved in the cycle for duplicating a typical reentry from a lunar mission are low enough for existing pressure-vessel techniques. Both the known and anticipated advantages and disadvantages of this new concept are also discussed.*


## INTRODUCTION

An appreciation of the magnitude of the problem facing the designer of an experimental facility capable of duplicating the environment of a space vehicle reentering the earth's atmosphere may be obtained by inspection of figure 1. On this altitude-velocity diagram there is a curve designated as "Lunar reentry" computed for the $10g$ limited undershoot of a nonlifting vehicle having a ballistic parameter $W/C_DA$ of 50 lb/sq ft. Although an actual lunar vehicle will probably be a lifting configuration, this typical trajectory adequately serves as a guide to the requirements

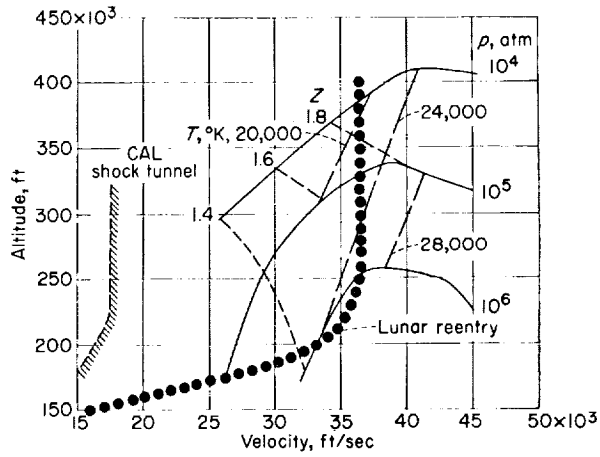


FIGURE 1.—Stagnation temperature, pressure, and compressibility factor required for isentropic expansion to duplicate velocities at ambient altitude conditions. A nonlifting $10g$ undershoot lunar return trajectory is shown for $\frac{W}{C_DA}=50$ lb/sq ft.

[1] After submission of this report for publication the author learned that E. L. Resler and D. E. Bloxsom at the Cornell University Graduate School of Aeronautical Engineering had earlier (1952) propounded a similar device for perfect gases in a short monograph having limited distribution. Their proposal was subsequently briefly treated as part of a general survey by A. Hertzberg, W. E. Smith, H. S. Glick, and W. Squire of Cornell Aeronautical Laboratory in AEDC-TN-55-15 (AD-789-A-2).

for a testing environment. Plotted on the figure are lines of constant reservoir or stagnation temperature, pressure, and compressibility for an equilibrium isentropic expansion to the ambient altitude conditions at a given velocity. (These curves are for illustrative purposes only, since extensive extrapolation was required in their construction.) In the critical heating period which occurs near the "knee" of the trajectory, stagnation pressures in excess of a million atmospheres and temperatures above 25,000° K, with dissociation greater than 50 percent, are required. It is of interest to note that over 10 megawatts of power per square foot of test-section area would be expended during the operation of a facility in this altitude-velocity region. Since present-day pressure-vessel technology halts two orders of magnitude below these stagnation pressures, it is obvious that no facility (either continuous or intermittent) attaining these stagnation conditions during its thermodynamic processes will be constructed in the near future. Arc, "hot shot," and reflected-shock tunnels are all facilities in this category requiring stagnation conditions during their operating cycle.

Duplication of the ambient atmospheric conditions, as well as the velocity, in an experimental facility becomes a necessity as the reentry speeds under study increase. The reasons for duplication rather than simulation (i.e., the matching of conditions at only certain points of the flow) may be demonstrated by comparing some of the primary heating problems of entry from hyperbolic orbits with those of suborbital reentry.

As an example of the latter type, consider the reentry of an ICBM nose cone. Shock tubes were very successful in determining the convective heating rates applicable to the ICBM heat shield by a simulation wherein the gas conditions in the stagnation region behind the detached bow shock were selected to match those of the nose cone in atmospheric flight, while the ambient conditions (ahead of the shock) were drastically different. In free flight almost all of the free-stream energy is kinetic, but in the shock tube the energy is nearly equally divided between kinetic and thermal forms, with the result that the shock tube Mach number is low. However, for these blunt nonlifting nose shapes the velocity distribution on the heat shield is fortunately insensitive to free-stream Mach number, and thus the convective heating in this region was satisfactorily obtained.

Now consider the different problems of spacecraft reentry. As reentry velocity increases, the heating due to radiation from the air behind the shock wave, which varies in proportion to the velocity raised to a large power, becomes very important and for blunt shapes will overshadow the convective heating. This radiation may be treated as two types, equilibrium and nonequilibrium. The latter type arises because different numbers of molecular collisions are required to activate the different energy levels. Consequently, the energy first goes into those levels most easily activated and then is redistributed by subsequent collisions until the equilibrium state is reached. The temperature and composition of the gas before equilibrium is reached result in radiation designated as nonequilibrium radiation. Since the nonequilibrium radiation is dependent on the successive states of the gas, it is obvious that if an experiment is to reproduce the successive states of atmospheric flight it must necessarily start from the same state or ambient free-stream conditions. Consequently, the shock-tube simulation of only stagnation conditions behind a normal shock is not sufficient in this case.

Equilibrium radiation also depends upon the state and volume of the radiating gas behind the bow shock wave. This volume is dependent on the shock detachment distance, which is in turn dependent on the density ratio across the shock wave. Consequently, the requirement of equal density ratios reintroduces the necessity for equal ambient conditions for equilibrium radiation testing also.

Lifting vehicles will be considered for manned reentry from space flight because of deceleration and heating alleviation as well as landing range gains. Since for such lifting vehicles the convective heating rates at points other than the stagnation region are important and since these rates are dependent on free-stream Mach number as well as on enthalpy, the simulation afforded by the shock tube is no longer sufficient even for convective heating.

While the shock tube and shock tunnel were the experimental "workhorses" for the ICBM and

hypersonic-glider studies in the velocity range of 20,000 ft/sec and below, these facilities fall far short of the performance required for studies in the critical regions of lunar reentry. An idea of the present-day limit on shock-tunnel operation is the boundary labeled "CAL shock tunnel" in figure 1, which represents the performance expected from Cornell Aeronautical Laboratory's new 6-foot shock tunnel (ref. 1). Furthermore, even if the shock tunnels had the pressure-enthalpy (altitude-velocity) potential, they would be faced with the serious problem of nonequilibrium dissociated flow in the test section due to the freezing (i.e., recombination of atoms approaching zero) of the rapidly expanding flow in the nozzle (ref. 1).

Useful data regarding nonequilibrium radiation occurring behind the bow shock wave of bodies traveling at high velocity and high altitudes have been obtained in two different ways. At the Avco-Everett Research Laboratory a low-density shock tube was employed to study only the relaxation and radiation processes behind a normal shock moving into still air (ref. 2). At the Ames Research Center a small projectile was launched against the flow of a shock tunnel to study the integrated thermal radiation at high velocities (ref. 3). The data obtained from these facilities have significantly enhanced the understanding of the reentry problem; yet they leave wide voids in the picture since the Avco technique gives results only for normal-shock radiation and the Ames technique is presently limited to small models with no onboard radiation instrumentation.

Consequently, an urgent need now exists for a new type of facility capable of duplicating the altitude-velocity requirements of the return from a lunar mission. In the near future a facility will be needed that is capable of satisfying the even more stringent requirements of interplanetary probes, both reentering the earth's atmosphere and entering other planetary atmospheres. The latter requirement necessitates the use of testing mediums other than air.

A preliminary theoretical investigation of a new facility concept with the aforementioned capabilities is contained in this report. This facility utilizes unsteady wave processes for total-enthalpy multiplication.

Only minimum referencing will be found herein, and in many cases a single reference is used to illustrate a point on which many reports have been written. This procedure has been followed because hundreds of papers pertinent to various aspects of unsteady flows and shock tunnels have been written. Additional background information may be found, for example, in the works listed in the extensive bibliographies of references 1 and 4.

## SYMBOLS

| | |
|---|---|
| $A$ | cross-sectional area of expansion tube, or reference area of reentry vehicle, sq ft |
| $a$ | velocity of sound, ft/sec |
| $B, C$ | constants in linearized relation between velocity of sound and enthalpy (appendix B) |
| $C_D$ | drag coefficient of reentry vehicle |
| $c_p$ | specific heat at constant pressure |
| $c_v$ | specific heat at constant volume |
| $E$ | arc energy, joules |
| $g$ | acceleration due to gravity |
| $H$ | total enthalpy |
| $h$ | local enthalpy |
| $h^*$ | value of local enthalpy at lower limit of linear relation (appendix B) |
| $l_D$ | length of driver section of expansion tube |
| $l_{s_1}$ | length of driven section of expansion tube |
| $l_{s_2}$ | length of expansion section of expansion tube |
| $M$ | flow Mach number |
| $M_{s_1}$ | Mach number of primary shock wave |
| $M_{s_2}$ | Mach number of secondary shock wave |
| $p$ | absolute pressure |
| $R$ | gas constant per unit mass |
| $R_{univ}$ | gas constant per mole |
| $S_1$ | primary shock wave |
| $S_2$ | secondary shock wave |
| $s$ | entropy per unit mass |
| $T$ | absolute temperature |
| $T_{t,2}$ | perfect-gas total temperature behind shock wave |
| $t$ | time |
| $\Delta t$ | nominal testing time (time between passage of entropy discontinuity and arrival of expansion fan at test section) |

| | |
|---|---|
| $U_{S_1}$ | velocity of primary shock wave |
| $U_{S_r}$ | velocity of reflected shock wave |
| $u$ | velocity of fluid |
| $W$ | weight of reentry vehicle, lb |
| $W/C_DA$ | ballistic parameter, lb/sq ft |
| $Z$ | compressibility factor, $p/\rho RT$ |
| $\alpha$ | function defined in equation (B4a) |
| $\gamma$ | ratio of specific heats, $c_p/c_v$ |
| $\gamma_e$ | effective ratio of specific heats |
| $\rho$ | density |

Subscripts:

| | |
|---|---|
| $ET$ | expansion tube |
| $NRS$ | nonreflected-shock tunnel |
| $RS$ | reflected-shock tunnel |
| $o$ | standard conditions |
| 1, 2, 3, 4 | conditions in expansion tube (fig. 2(a)) and corresponding conditions in shock tunnel |
| 5 | test-section conditions |
| 6 | stagnation conditions behind reflected shock wave |
| 10, 20 | conditions in expansion tube (fig. 2(a)) |

## DESCRIPTION AND OPERATING CYCLE OF EXPANSION TUBE

The proposed simple expansion tube is shown schematically in figure 2. It is similar in many respects to a shock tunnel, but has a major difference in that the steady-flow varying-area-nozzle expansion of the shock tunnel is replaced by a nonsteady constant-area expansion. The apparatus is divided by two diaphragms into three sections. The driver or high-pressure section contains a gas at high pressure and high speed of sound. The driven section is filled with the gas in which the testing is to be performed. The expansion or accelerating section is filled with an accelerating light gas at very low pressure. A diaphragm capable of withstanding high pressures separates the driver and driven sections; a weak low-pressure diaphragm separates the driven and expansion sections. The test section and model are located near the downstream end of the expansion section.

The operating sequence commences when the rupture of the high-pressure diaphragm propagates a primary shock wave $S_1$ into the test gas and an expansion wave into the driver gas. (See fig. 2(c).) The shock wave $S_1$ then encounters and ruptures the low-pressure diaphragm. A new secondary shock wave $S_2$ propagates into the accelerating light gas while an upstream expansion wave moves into the test gas (fig. 2(d)). This expansion wave is washed downstream since region ② is supersonic. The test region is the area ⑤ in figures 2(a) and 2(e), between the entropy discontinuity and the trailing edge of the expansion fan.

## THEORY

The basis which enables the expansion tube to outperform conventional shock tunnels may be explained by the two simple equations for expansion of the testing medium. The equation for the shock-tunnel nozzle is that of a steady isentropic expansion,

$$du=-\left(\frac{dh}{u}\right)_s \tag{1a}$$

while the equation for the expansion tube is the unsteady wave expansion,

$$du=-\left(\frac{dh}{a}\right)_s \tag{1b}$$

From these equations the total-enthalpy change of the stream is found to be

$$dH=0 \tag{2a}$$

for the steady case and

$$dH=-(M-1)dh \tag{2b}$$

for the unsteady case.

Thus it is obvious that to attain high values of $u$ for hypersonic testing ($u \gg a$, $M \gg 1$) the unsteady expansion is much more efficient for two reasons. First, in the unsteady expansion the velocity increment added for a given reduction in static enthalpy is greater by a factor of $M$ (compare eqs. (1)). Second, the flow processes are such as to actually increase the total enthalpy in the unsteady expansion by large amounts for $M \gg 1$; in other words, the isentropic unsteady expansion wave is a total-energy multiplier when the total energy is measured in a fixed reference frame.

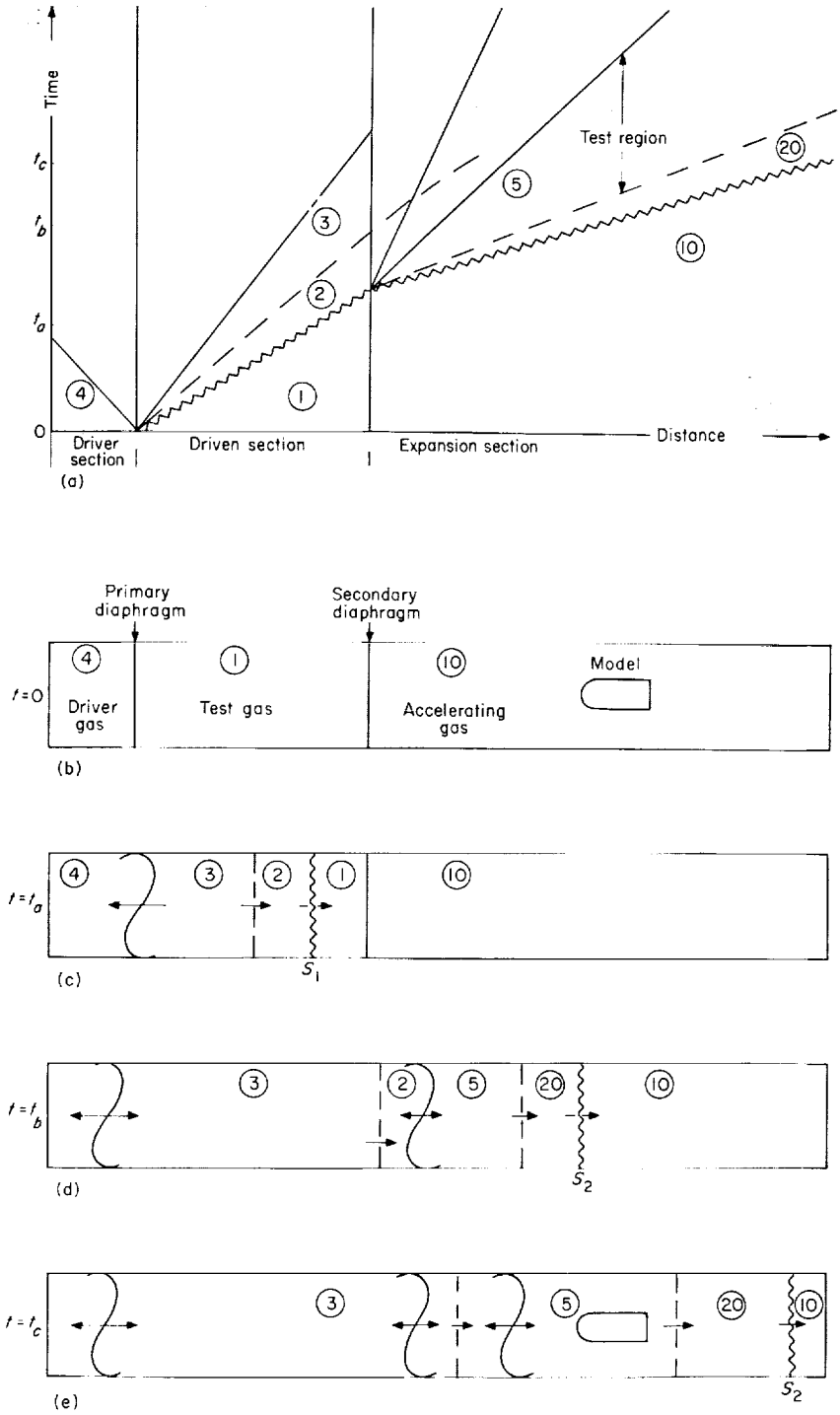


(a) Distance-time plot.
(b) Prior to run, $t=0$.
(c) After primary diaphragm burst, $t=t_a$.
(d) After secondary diaphragm burst, $t=t_b$.
(e) During testing, $t=t_c$.

FIGURE 2.—Sketches illustrating expansion-tube cycle.

### PERFECT-GAS ANALYSIS

The equations and performance of a perfect-gas expansion tube will be derived first, since closed-form equations can be obtained to illustrate the various benefits and advantages. The strong-shock approximations $\left(\frac{p_2}{p_1}\gg 1, \frac{p_{20}}{p_{10}}\gg 1\right)$ are employed because all operating conditions of interest require a strong shock. Equations (3) to (6) then apply for perfect gases:

$$\frac{u_2}{a_1}\approx\sqrt{\frac{2}{\gamma_1(\gamma_1+1)}\frac{p_2}{p_1}} \tag{3}$$

$$\frac{a_2}{a_1}\approx\sqrt{\frac{\gamma_1-1}{\gamma_1+1}\frac{p_2}{p_1}}\approx\sqrt{\frac{\gamma_1(\gamma_1-1)}{2}}\frac{u_2}{a_1} \tag{4}$$

$$M_2\approx\sqrt{\frac{2}{\gamma_1(\gamma_1-1)}} \tag{5}$$

$$M_{s_1}\equiv\frac{U_{s_1}}{a_1}\approx\sqrt{\frac{\gamma_1+1}{2\gamma_1}\frac{p_2}{p_1}}\approx\frac{\gamma_1+1}{2}\frac{u_2}{a_1} \tag{6}$$

These equations are also appropriate to the shock $S_2$ by substitution of subscripts 10 and 20 for 1 and 2.

Integration of equation (1b) for a perfect gas gives

$$\frac{2}{\gamma_1-1}a_2+u_2=\frac{2}{\gamma_1-1}a_5+u_5 \tag{7}$$

$$\frac{a_5}{a_2}=\frac{1+\frac{\gamma_1-1}{2}M_2}{1+\frac{\gamma_1-1}{2}M_5}\approx\frac{1+\sqrt{\frac{\gamma_1-1}{2\gamma_1}}}{1+\frac{\gamma_1-1}{2}M_5} \tag{8}$$

Now:

$$\frac{a_5}{a_1}=\frac{a_5}{a_2}\frac{a_2}{a_1}$$

$$\approx\frac{1+\sqrt{\frac{\gamma_1-1}{2\gamma_1}}}{1+\frac{\gamma_1-1}{2}M_5}\sqrt{\frac{\gamma_1-1}{\gamma_1+1}\frac{p_2}{p_1}} \tag{9}$$

Consequently, the required shock pressure ratio for given test condition $M_5$ is

$$\frac{p_2}{p_1}\approx\frac{\gamma_1+1}{\gamma_1-1}\left(\frac{1+\frac{\gamma_1-1}{2}M_5}{1+\sqrt{\frac{\gamma_1-1}{2\gamma_1}}}\right)^2\left(\frac{a_5}{a_1}\right)^2 \tag{10}$$

Also, the initial pressure in the driven chamber becomes

$$\frac{p_1}{p_5}=\frac{p_1}{p_2}\frac{p_2}{p_5}$$

$$=\frac{p_1}{p_2}\left(\frac{a_2}{a_5}\right)^{\frac{2\gamma_1}{\gamma_1-1}} \tag{11}$$

$$\approx\frac{\gamma_1-1}{\gamma_1+1}\left(\frac{1+\frac{\gamma_1-1}{2}M_5}{1+\sqrt{\frac{\gamma_1-1}{2\gamma_1}}}\right)^{\frac{2}{\gamma_1-1}}\left(\frac{a_1}{a_5}\right)^2 \tag{11a}$$

A plot of primary-shock pressure ratio $\frac{p_2}{p_1}$ against $\frac{p_1}{p_5}$ in an expansion tube for $\gamma=1.4$ and $a_1=a_5$ is given in figure 3. The test-section Mach numbers are indicated on the curve. Also shown is the performance of reflected- and nonreflected-shock tunnels. (See appendix A for pertinent equations.) The nonreflected-shock tunnel and expansion tube have coincident curves because the entropy increase of both flow systems is identical; however, at any point on the curve the value of $M_5$ in the expansion tube greatly exceeds the value in the nonreflected-shock tunnel. For example, for the same conditions of $\frac{p_2}{p_1}$ and $\frac{p_1}{p_5}$, $M_5\approx 42$ in the expansion tube and only 20 in the nonreflected-shock tunnel.

The gains that are theoretically realizable may be evaluated by comparing the pressure ratios required to match test-section conditions in the expansion tube to those in the shock tunnels. The ratios of $\frac{p_2}{p_1}$ are found from equations (10), (A5a), and (A8), and those of $\frac{p_1}{p_5}$ from equations (11a), (A6a), and (A9a).

$$\frac{\left(\frac{p_2}{p_1}\right)_{NRS}}{\left(\frac{p_2}{p_1}\right)_{ET}}\approx\frac{\gamma_1}{\gamma_1+1}\left(1+\sqrt{\frac{\gamma_1-1}{2\gamma_1}}\right)^2\frac{1+\frac{\gamma_1-1}{2}M_5^2}{\left(1+\frac{\gamma_1-1}{2}M_5\right)^2} \tag{12}$$

$$\frac{\left(\frac{p_2}{p_1}\right)_{RS}}{\left(\frac{p_2}{p_1}\right)_{ET}}\approx\frac{\gamma_1}{3\gamma_1-1}\left(1+\sqrt{\frac{\gamma_1-1}{2\gamma_1}}\right)^2\frac{1+\frac{\gamma_1-1}{2}M_5^2}{\left(1+\frac{\gamma_1-1}{2}M_5\right)^2} \tag{13}$$

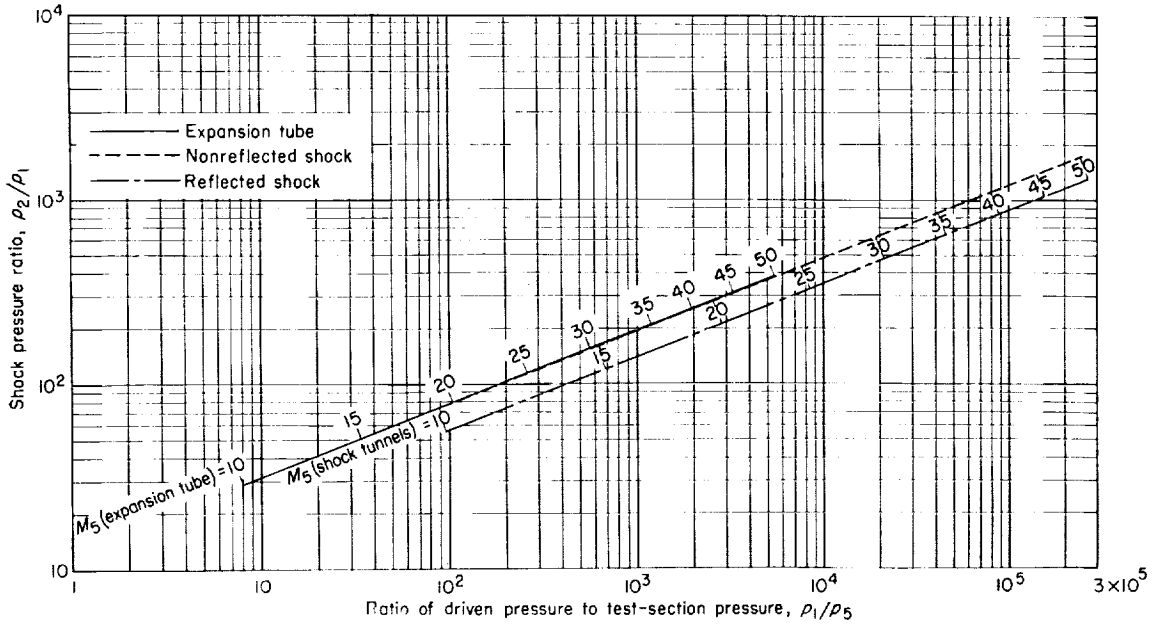


FIGURE 3.—Perfect-gas nondimensional performance curves for expansion tube and shock tunnels. $M_5$ is the test Mach number. $a_1=a_5$; $\gamma=1.4$.

$$\frac{(p_1)_{NRS}}{(p_1)_{ET}} \approx \left(\frac{\gamma_1}{\gamma_1+1}\right)^{\frac{1}{\gamma_1-1}} \left(1+\sqrt{\frac{\gamma_1-1}{2\gamma_1}}\right)^{\frac{2}{\gamma_1-1}} \left[\frac{1+\frac{\gamma_1-1}{2}M_5^2}{\left(1+\frac{\gamma_1-1}{2}M_5\right)^2}\right]^{\frac{1}{\gamma_1-1}} \tag{14}$$

$$\frac{(p_1)_{RS}}{(p_1)_{ET}} \approx \frac{\gamma_1-1}{\gamma_1}\left(1+\sqrt{\frac{\gamma_1-1}{2\gamma_1}}\right)^{\frac{2}{\gamma_1-1}} \left[\frac{1+\frac{\gamma_1-1}{2}M_5^2}{\left(1+\frac{\gamma_1-1}{2}M_5\right)^2}\right]^{\frac{1}{\gamma_1-1}} \tag{15}$$

These ratios are plotted in figure 4, and together show the advantages of the expansion tube. Not only is the shock pressure ratio $\frac{p_2}{p_1}$ greater for the shock tunnels, but also the pressure $p_1$ into which the shock must propagate is higher. The asymptotic levels for $M_5 \to \infty$ are 5.5 and 4.2 for equations (12) and (13), and 72.2 and 79.4 for equations (14) and (15).

The gains of the expansion tube are mainly due to the total-enthalpy increase effected by the expansion wave between regions ② and ⑤. The

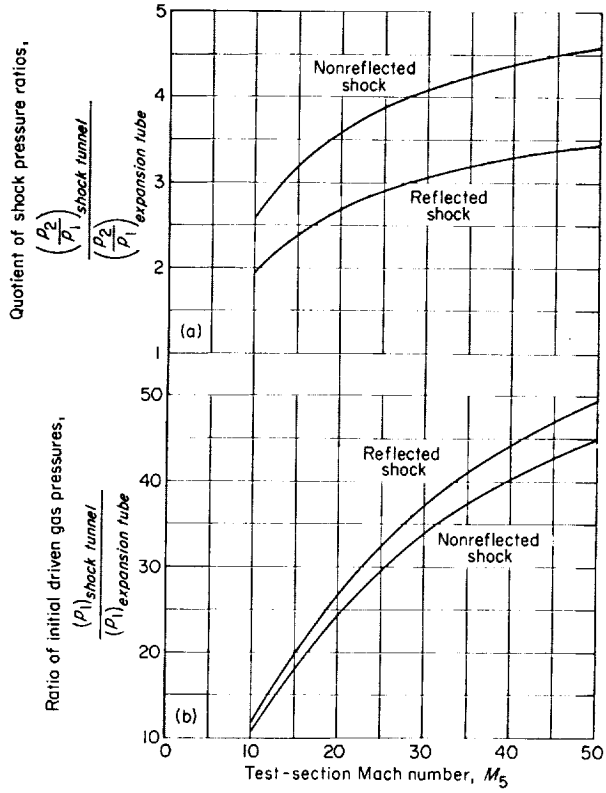


(a) Shock pressure ratio.
(b) Initial driven pressure.

FIGURE 4.—Comparison of perfect-gas shock pressure ratios and initial driven-chamber pressures for same test-section $M_5$ and $p_5$ in expansion tube and shock tunnels.

ratio of total enthalpies $\frac{H_5}{H_2}$ can be expressed as

$$\left(\frac{H_5}{H_2}\right)_{ET} \approx \frac{\gamma_1-1}{2(\gamma_1+1)}\left(1+\sqrt{\frac{2\gamma_1}{\gamma_1-1}}\right)^2 \frac{1+\frac{\gamma_1-1}{2}M_5^2}{\left(1+\frac{\gamma_1-1}{2}M_5\right)^2} \tag{16}$$

For $\gamma_1=1.40$, this ratio approaches 5.54 as $M_5\to\infty$, and more than 80 percent of the final total enthalpy is added in the expansion process. It is for this reason that the apparatus has been called an expansion tube. In the nonreflected-shock tunnel $\frac{H_5}{H_2}=1$, whereas in the reflected-shock tunnel $\frac{H_5}{H_2}=\frac{H_6}{H_2}\approx\frac{3\gamma_1-1}{\gamma_1+1}=\frac{4}{3}$, for $\gamma_1=1.40$; thus the reflected shock increases the enthalpy by approximately 33 percent.

### REAL-AIR ANALYSIS

**Computational procedure.**—For the case of real air as a test medium the expansion and shock processes can no longer be treated in closed form. Instead, the air is assumed to be in equilibrium and Mollier diagrams (refs. 5 and 6) are employed to determine the subsequent states of the air during the processes.

A reverse integration procedure was employed for these real-air solutions. The final test conditions of velocity ($u_5$) and altitude ($p_5$, $s_5$) were first selected, and then the required extent of the expansion fan, shock-wave strength, and initial pressure $p_1$ were determined. A detailed outline of the procedure is given in appendix B. Approximations were introduced to facilitate the solution, but it is estimated that the errors so introduced are under 2 percent in any quantity. The initial temperature $T_1$ was chosen as 300° K and the model atmosphere of reference 7 was selected for ambient conditions.

Solutions were obtained for altitudes and velocities of interest for reentry from lunar or near-space missions. The altitudes selected were 250,000, 200,000, 150,000, and 100,000 feet and solutions were found for velocities of 20,000, 30,000, 33,000, and 40,000 ft/sec. Solutions were not obtained for the two higher velocities at 100,000 feet because the state ② required was not on available Mollier diagrams. The speed of sound in state ① was $a_1=1{,}142$ ft/sec.

**Nondimensional results.**—The real-air counterpart of figure 3 appears as figure 5, where the shock pressure ratio $\frac{p_2}{p_1}$ is plotted against $\frac{p_1}{p_5}$. Perfect-gas curves are also shown for $\frac{a_5}{a_1}=1.0$ and 0.91. The real-air curves do not coincide for two reasons, the imperfect-gas effect and the different speeds of sound for the different altitudes. Note that although the curves are not sequential in regard to altitude they are sequential in regard to $\frac{a_5}{a_1}$, and in the order indicated by the two perfect-gas curves. An interesting result is that the real-gas curves require a lower $\frac{p_2}{p_1}$ than the perfect gas at the same value of $M_5$. For example, when $u_5=$ 33,000 ft/sec at an altitude of 150,000 feet, $M_5=30$ and $\frac{p_2}{p_1}\approx 125$ for the real gas. The perfect-gas value of $\frac{p_2}{p_1}$ is approximately 150 for $M_5\approx 30$ and the same value of $\frac{a_5}{a_1}$.

In figure 6 the shock Mach number $M_{s_1}$ is plotted against the test-section Mach number $M_5$ for the expansion tube with both real and perfect air and for the nonreflected-shock tunnel with real air. Approximate operating characteristics of the expansion tube for other altitudes and velocities may be obtained from interpolation (on a velocity-of-sound basis) of figures 5 and 6 in the nondimensional form presented. Figure 7 shows the total-enthalpy multiplication factor of the expansion fan. The ordinate $\frac{H_5}{H_2}$ is approximately equal to $\frac{(u_5)^2_{ET}}{(u_5)^2_{NRS}}$ since $h_5$ will be negligible. The perfect-gas curve is independent of $\frac{a_5}{a_1}$, and the real-gas data are practically on a common curve. Figures 6 and 7 prove that the large gains of the expansion tube over the shock tunnel predicted by perfect-gas theory are not only realized but exceeded with the real gas. The comparison is made with the nonreflected-shock tunnel; however, for the same high-temperature driver, reflected-shock performance is slightly better than nonreflected for perfect air and slightly worse for real air. Furthermore, the effectiveness increases with Mach number (as would be expected from eqs. (1) and (2)).

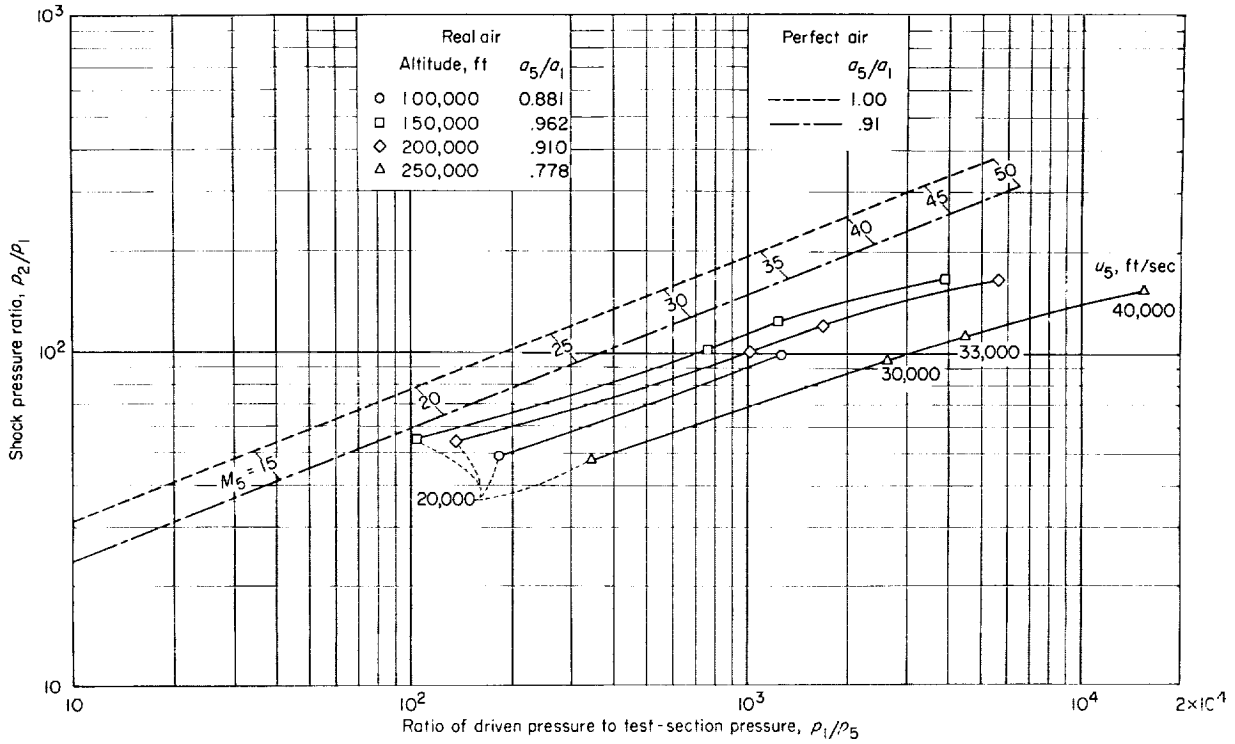


FIGURE 5.—Nondimensional performance curves for expansion tube. The perfect-air curves are computed for two values of $\frac{a_5}{a_1}$ and $\gamma=1.4$. The real-air curves are for $a_1=1{,}142$ ft/sec.

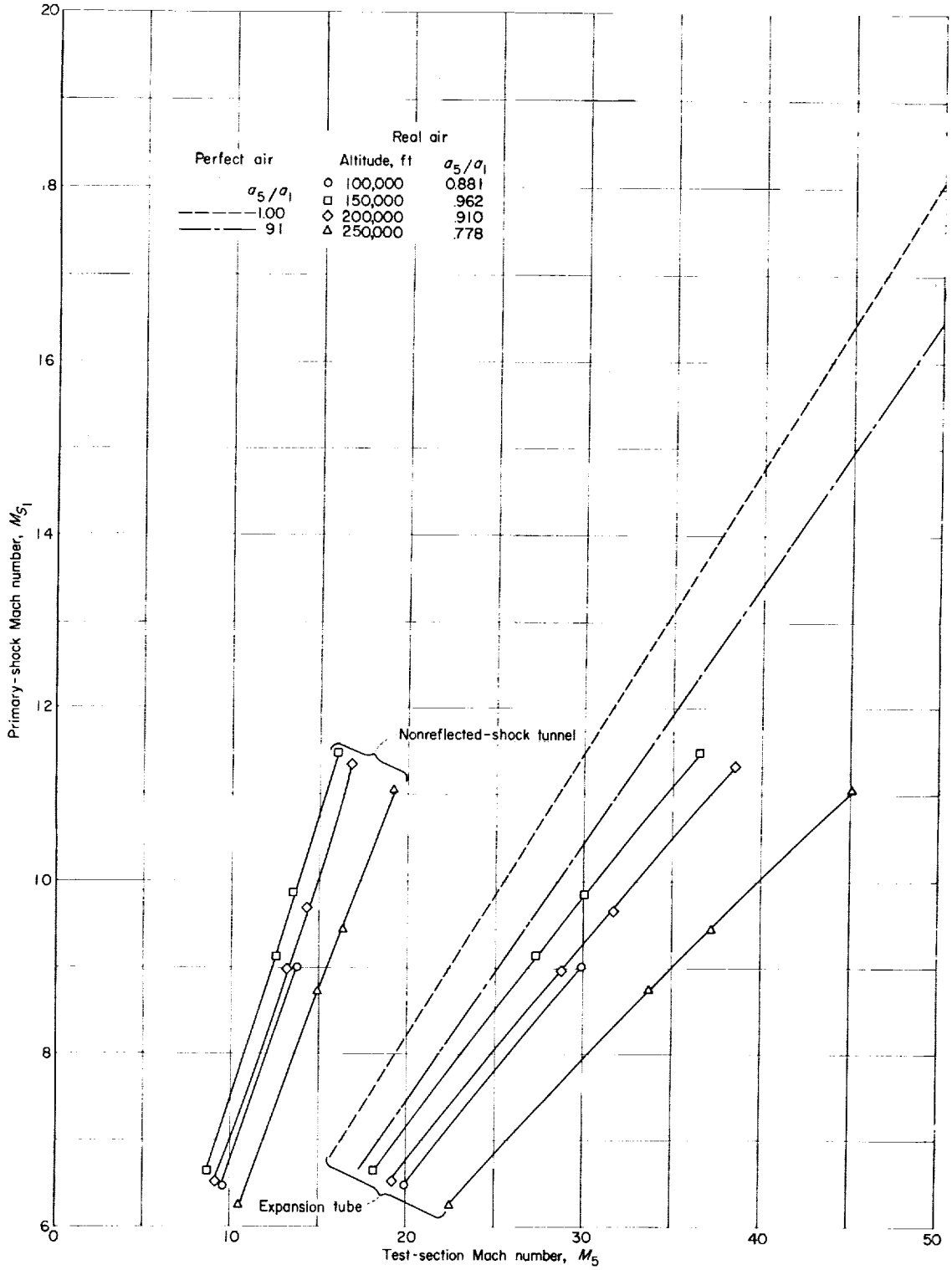


FIGURE 6.—Curves of primary-shock Mach number against test-section Mach number for expansion tube and nonreflected-shock tunnel.

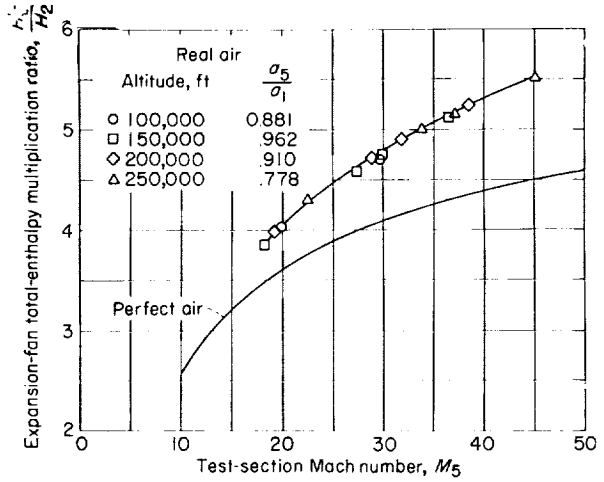


FIGURE 7.— Total-enthalpy multiplication in expansion fan of expansion tube.

## DESIGN CONSIDERATIONS

### THERMODYNAMIC STATES OF EXPANSION-TUBE CYCLE

**Test gas.**—In order to design an expansion tube it is necessary to know the absolute magnitudes of the pressures involved. These are shown for the selected altitudes in figures 8 and 9 for initial driven-chamber pressure $p_1$ and pressure behind the primary shock $p_2$. Two units are employed for these and all subsequent pressure ordinates; the left-hand scale is in standard atmospheres and the right-hand scale in the units most appropriate to the particular pressure level (mm Hg, lb/sq in. abs, or $\mu$ Hg). The $10g$ nonlifting undershoot for the vehicle with $W/C_DA=50$ lb/sq ft is indicated by the heavy dotted lines.

The value of $p_1$ in figure 8 ranges from 5 mm Hg to $10^4$ mm Hg, but the typical lunar return trajectory only requires an upper limit on $p_1$ of approximately 300 mm Hg. Thus a weak diaphragm is sufficient to separate states ① and ⑩. Similarly, the extreme values of $p_2$ shown in figure 9 are not required for the lunar mission, a maximum of 700 lb/sq in. abs being sufficient.

The compressibility factor $Z_2$ is plotted in figure 10. A comparison of figures 1 and 10 shows that the expansion tube operates with much less dissociation ($Z_2-1$) than the reflected-shock tunnel. For example, at an altitude of 200,000 feet on the typical lunar reentry trajectory the maximum dissociation in the air cycle would be about 45 percent for the reflected-shock tunnel and only 5 percent in the expansion tube. Thus even if the flow were to "freeze" in the expansion tube, only a small part of the energy would be out of equilibrium.

However, the possibility of maintaining an equilibrium flow appears good for the expansion tube. Except near the origin of the expansion fan, where the air is expanded very rapidly, the expansion processes are relatively spread out over a long part of the expansion chamber. For hypersonic testing the minimum and maximum spatial extent of the expansion processes associated with a particular element of gas are as follows. The minimum is 0 percent of the accelerating chamber length for the gas which is expanded discontinuously at the origin of the expansion fan. The maximum is over 99 percent of the accelerating chamber length for the gas reaching the test section concurrently with the trailing edge of the expansion fan (i.e., at the termination of the test region ⑤). Since the accelerating-chamber lengths will be shown to be of the order of hundreds of feet, compared with the shock-tunnel nozzle lengths of the order of tens of feet, the possibility of attaining equilibrium appears more favorable for the former. An exception may be the part of the air processed near the fan origin, which may remain frozen even though it has a long distance in which to attempt to regain equilibrium (ref. 8).

**Accelerating gas.**—Conditions ⑩ for the accelerating light gas will now be considered. The pressure ratio $\frac{p_{20}}{p_{10}}$ for any gas may be evaluated as

$$\frac{p_{20}}{p_{10}}=1+\frac{u_{20}^2}{R_{10}T_{10}}\frac{1}{1-\frac{\rho_{10}}{\rho_{20}}} \tag{17}$$

$$=1+\frac{u_5^2}{T_{10}R_{univ}}\frac{(\text{mol. wt.})_{10}}{1-\frac{\rho_{10}}{\rho_{20}}} \tag{17a}$$

Consequently, to maximize $p_{10}$, since $p_{20}=p_5$ and $u_5$ are fixed, a gas with a low molecular weight and a high density-ratio potential $\frac{\rho_{20}}{\rho_{10}}$ is desirable. Hydrogen is the obvious choice if only these restrictions are considered. However, in view of the dangers associated with hydrogen usage, it is believed desirable to use helium for the accelerating chamber unless $p_{10}$ becomes too small for the vacuum pumping available. Consequently, results are presented for helium. It is assumed to be a perfect gas, and therefore equation (17a) reduces to equation (3).

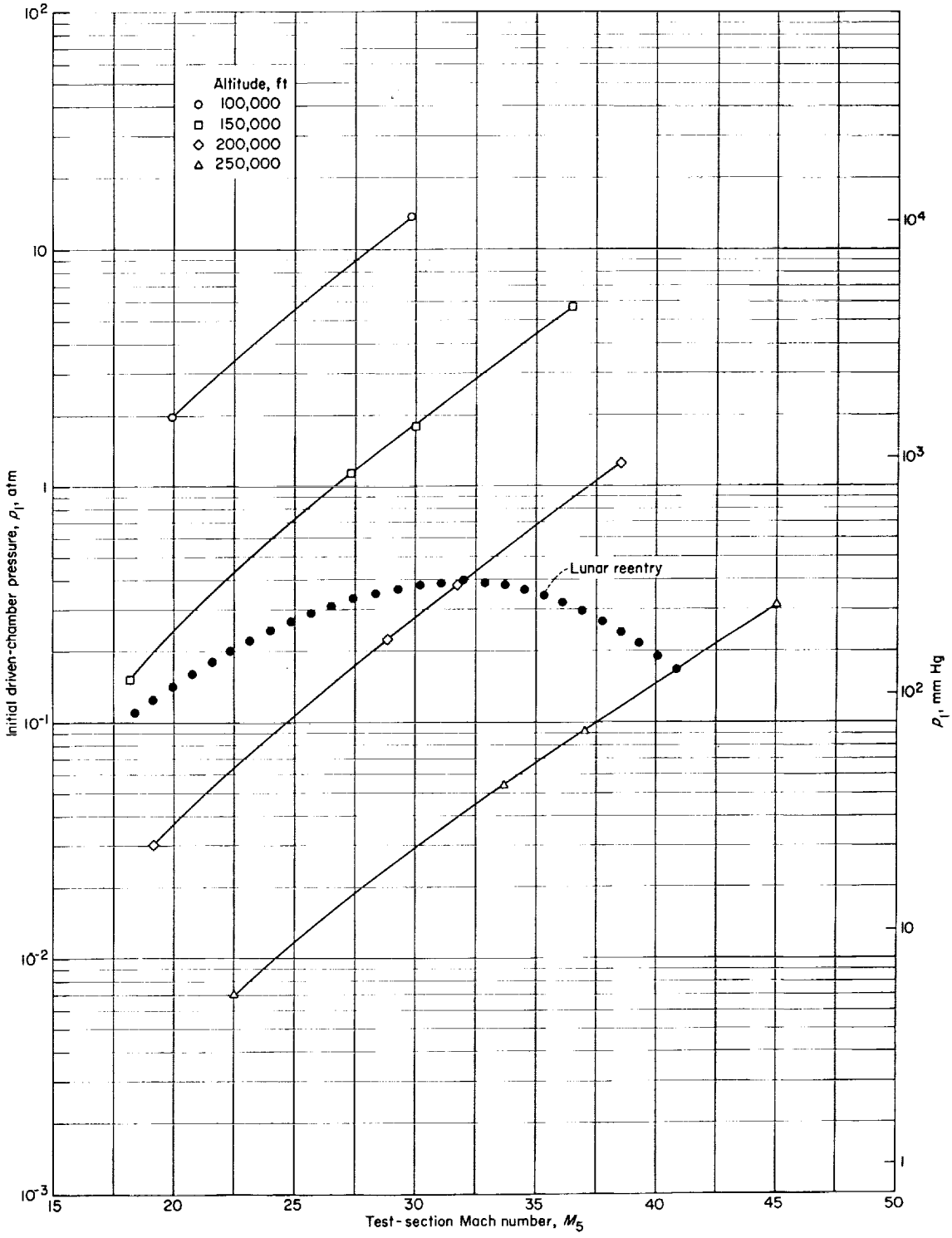


FIGURE 8.—Relation between initial driven-chamber pressure and test-section Mach number.

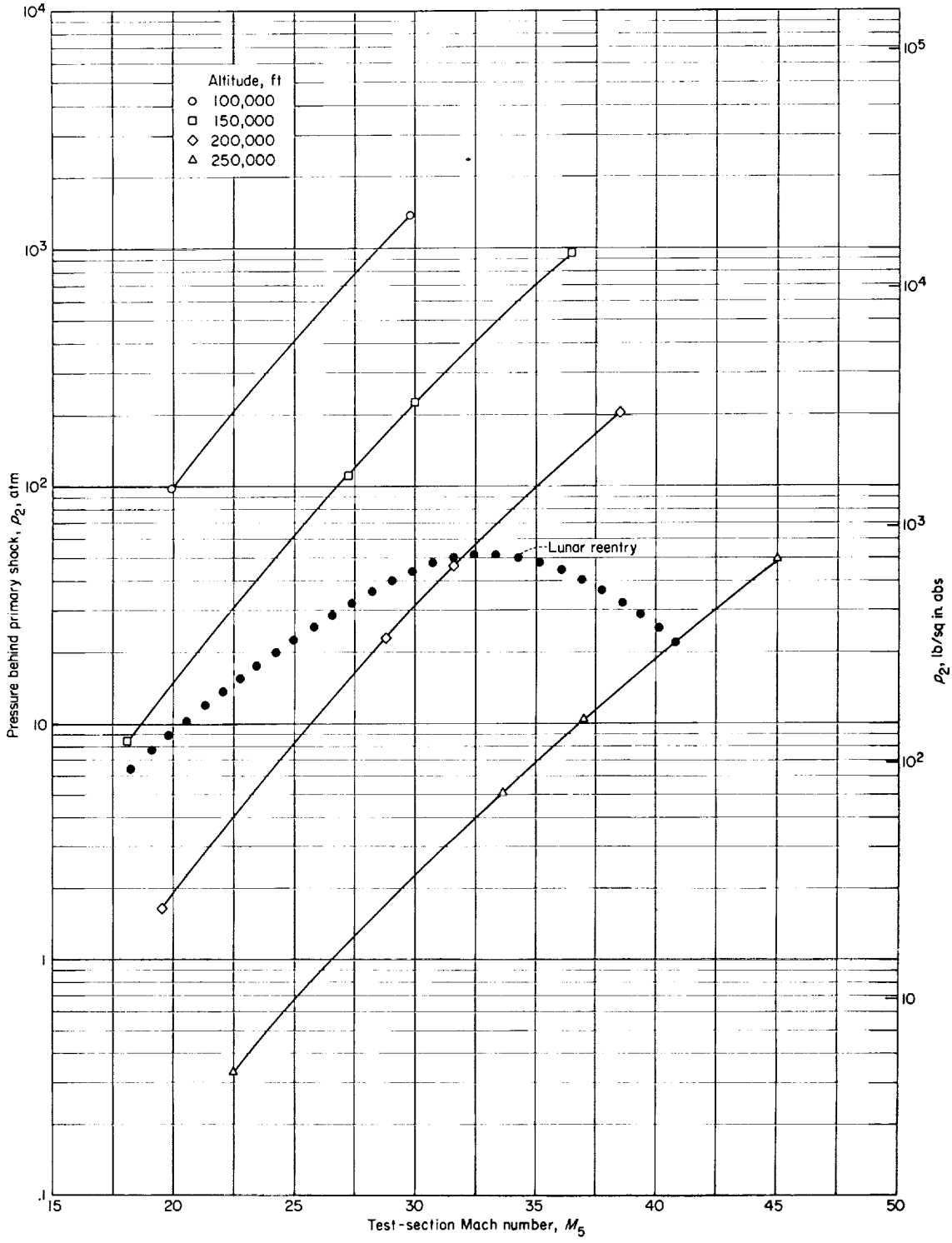


FIGURE 9.—Relation between pressure behind primary shock wave and test-section Mach number.

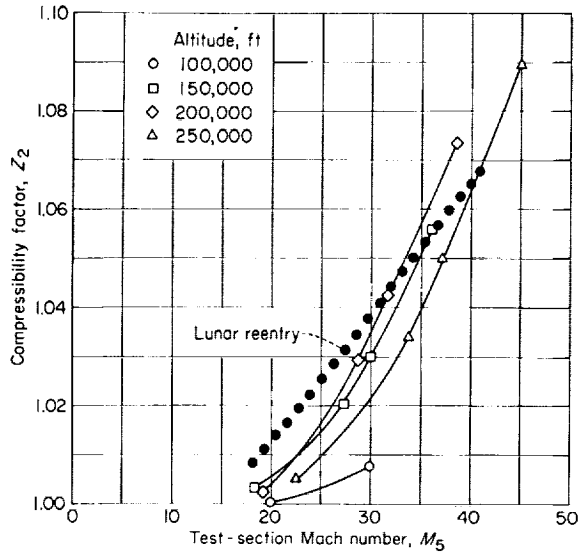


FIGURE 10.—Relation between compressibility factor behind primary shock wave and test-section Mach number.

Values of $p_{10}$ are plotted in figure 11 for initial temperatures $T_{10}$=273° and 300° K in helium. The minimum value of $p_{10}$ required for the typical lunar return is about 0.05 $\mu$ Hg.

**Driver gas.**—In this report only heated helium with a constant-area driver will be considered for the driver. More advantageous driver techniques such as varying area and buffered drivers will probably reduce the driver pressures; however, in this preliminary investigation these methods are not treated. (See ref. 9 for driver techniques for shock tubes.) Combustion of stoichiometric oxygen-hydrogen mixtures and electric-arc discharge are the methods investigated to heat the helium. Values of $a_4$ and $\gamma_4$ from reference 9 were used for the combustion drive with 75, 80, and 85 percent helium. For the arc drive, helium was assumed to be an un-ionized perfect gas heated to temperatures $T_4$ of 2,000°, 4,000°, 7,500°, and 10,000° K.

The driver state ④ is easily determined with the assumption that the process ④→③ is isentropic with a constant value of $\gamma$. (See refs. 4 and 9.) The pertinent equation is

$$\frac{p_4}{p_3}=\frac{p_4}{p_2}=\left(1-\frac{u_2}{a_4}\frac{\gamma_4-1}{2}\right)^{-\frac{2\gamma_4}{\gamma_4-1}} \tag{18}$$

The required driver pressures are plotted against test-section Mach number in figure 12(a) for arc drive and figure 12(b) for combustion drive. The lunar trajectory is shown for $T_4$=4,000° K in figure 12(a) and for 80 percent helium in figure 12(b). The driver pressure $p_4$ is relatively insensitive to $T_4$ (fig. 12(a)) because the advantages of high $T_4$ become more pronounced as $\frac{u_2}{a_4}$ becomes larger, and the values of $u_2$ are comparatively low in the expansion tube. The arc driver pressures are significantly lower than the combustion driver pressures for the same test conditions. Simulation of a typical lunar return trajectory would necessitate a maximum $p_4$ of about 3,700 lb/sq in. abs for the arc drive ($T_4$=4,000° K) and a maximum $p_4$ of about 8,200 lb/sq in. abs for combustion drive (80 percent helium). The use of high values of $T_4$ for an arc drive will be limited by both conductive and radiative heat loss to the walls of the driver chamber. Similarly, lower concentrations of helium in the combustion driver will be limited by detonation. Consequently, although lower driver pressures are ideally obtained by using higher $T_4$ (for arc drive) or lower helium percentage (for combustion drive), the aforementioned considerations may require operation at reduced values of $T_4$ or higher percentages of helium, which will result in driver pressures higher than optimum.

### LENGTHS OF COMPONENT SECTIONS

In the following paragraphs the lengths required of the various expansion-tube components are discussed. Again the problem is idealized because instantaneous diaphragm bursting and unmixed entropy discontinuities are assumed. Both perfect- and real-air results are presented simultaneously.

The lengths are nondimensionalized by dividing them by the standard speed of sound $a_o$ multiplied by the testing time $\Delta t$ in seconds between the passage of the helium-air entropy discontinuity (I in fig. 13) and the arrival of the expansion fan (II in fig. 13). The lengths of the driver and driven sections are optimized so that the reflected expansion wave from the closed end of the driver and the air-helium entropy discontinuity coalesce at the edge of the expansion fan (III in fig. 13). For real air the speed of sound is $a_1$=1,142 ft/sec. No details of the equations or computation scheme are given, since the integration along the characteristics is straightforward except that the linearized relation between $\frac{a}{a_o}$ and $\frac{h}{RT_o}$ was used for the accelerating expansion fan of the real air, and the driver gases had constant specific-heat ratios.

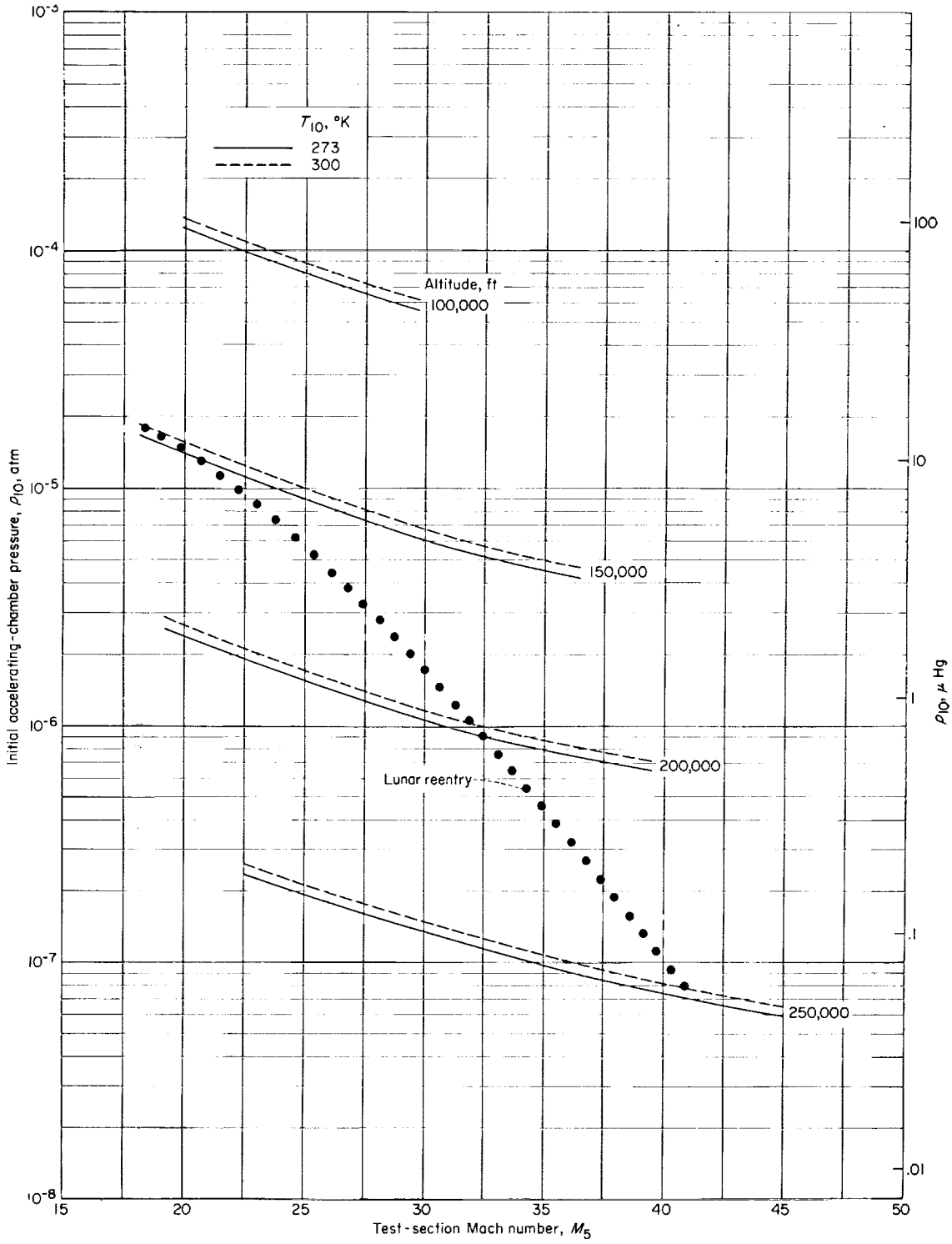


FIGURE 11.—Relation between initial pressure in accelerating chamber and test-section Mach number. The accelerating gas is helium and is assumed to be perfect.

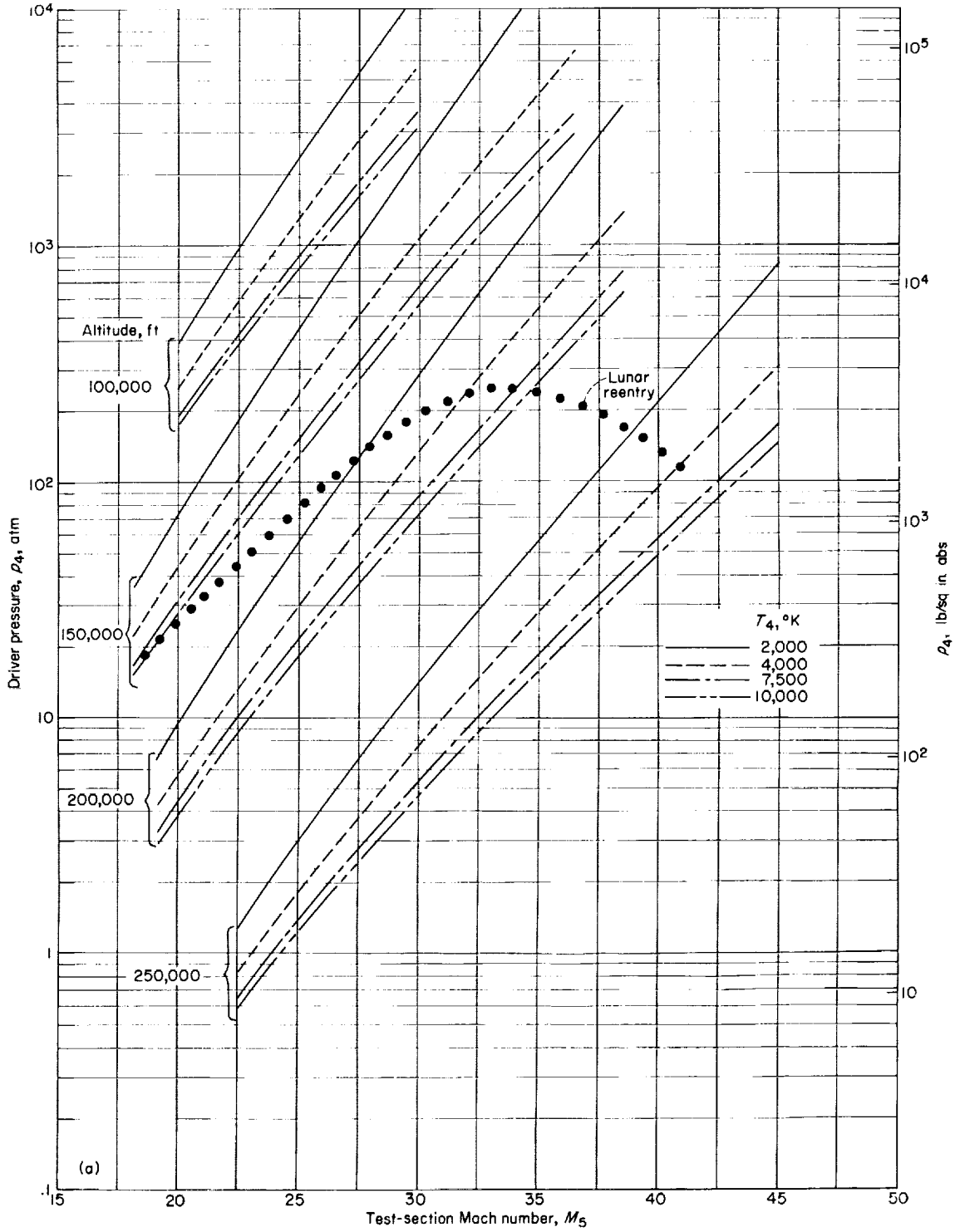


(a) Arc-heated helium drive. Lunar return plotted for $T_4 = 4{,}000°$ K.

FIGURE 12.—Relation between driver pressure and test-section Mach number for arc-heated helium and combustion drive.

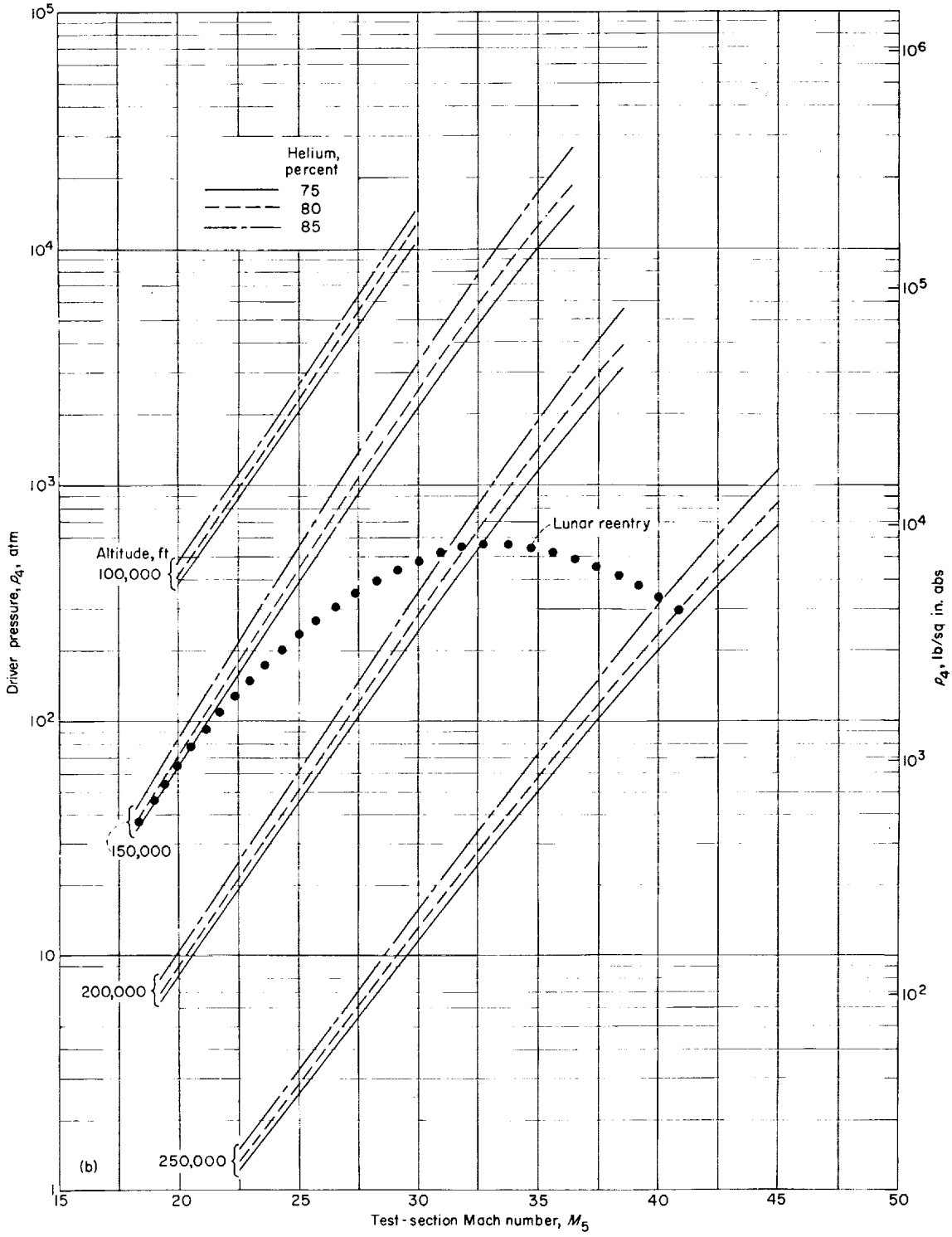


(b) Combustion drive. Lunar return plotted for 80 percent helium.

FIGURE 12.—Concluded.

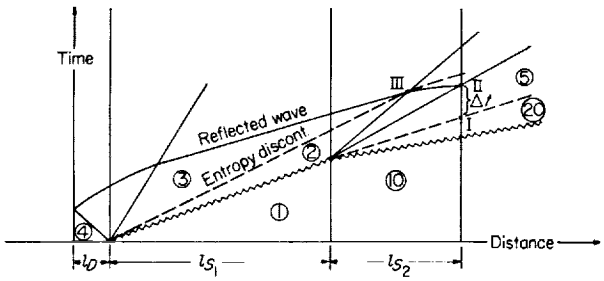


FIGURE 13.—Wave diagram of expansion tube illustrating determination of various section lengths.

**Accelerating-chamber length.**—An examination of figure 14, wherein $\frac{l_{s_2}}{a_o \Delta t}$ is plotted against $M_5$, reveals that the expansion tube suffers from the disadvantage common to shock tunnels in that long sections are required for even short testing times. For example, when $M_5 \approx 32$, the value of $\frac{l_{s_2}}{a_o \Delta t}$ is approximately 900 and an expansion-chamber length of about 1,000 feet would be needed for each millisecond of testing time. A comparison with conventional shock tunnels can be made for a lower test Mach number by using figure 3 of reference 1. For $M_5 \approx 18$, the values of $M_{s_1}$ required would be approximately 6¼, 12, and 11 for the expansion tube, nonreflected-shock tunnel, and tailored-interface reflected-shock tunnel, respectively. The nominal testing times (i.e., no allowance for the starting time of the shock-tunnel nozzles) in the nonreflected-shock tunnel would be about twice, and in the tailored-interface reflected-shock tunnel about twenty times, that in the expansion tube when the driven-chamber lengths of the shock tunnels are equal to the accelerating-chamber length of the expansion tube (these are the major lengths in both cases). The time expended in starting the shock tunnel nozzles will significantly reduce the foregoing factors.

**Driven-chamber length.**—The driven chambers are orders of magnitude shorter than the accelerating chambers for the same $M_5$. (See fig. 15.) The length $l_{s_1}$ decreases with increasing $M_5$, in contrast to $l_{s_2}$, with the net result that the ratio $\frac{l_{s_1}}{l_{s_2}}$ decreases from 0.02 to about 0.002 over the velocity and altitude range of figures 14 and 15.

**Driver-chamber length.**—The ratio of driver-chamber length $l_D$ to driven-chamber length $l_{s_1}$ is used in figure 16 rather than $\frac{l_D}{a_o \Delta t}$ for the following reason: The driver is "coupled" to the driven chamber regardless of the length $l_{s_2}$ or time $\Delta t$ because the driver must be of sufficient length to prevent the reflected expansion from overtaking the shock $S_1$ in the driven section. Thus, making $l_{s_1}$ greater than the value required by the curves of figure 15 would be harmful rather than beneficial if the driver length were not increased proportionately. The values of $l_D$ required (fig. 16(a)) decrease with the driver temperature $T_4$ because the velocity of sound $a_4$ decreases. For combustion drive (fig. 16(b)) the theoretical driver lengths are less than half the driven length, and consequently less than 1 percent of the expansion-chamber length $l_{s_2}$. Helium drivers are somewhat longer for the higher temperatures and vary in length from 150 percent to 10 percent of $l_{s_1}$.

**Dump-section length.**—A section is required downstream of the test section to delay the return to the test section of the reflection of the secondary shock. This section is the expansion-tube counterpart of the shock tunnel "dump tank." Perfect-gas computations indicate that if helium is the accelerating gas, a chamber with a diameter equal to that of the accelerating chamber and a length approximately one-ninth the length of the accelerating chamber should be sufficient to delay the shock reflection until time II of figure 13. Probably this length should be increased somewhat to allow for the boundary-layer growth through the reflected shock.

### ENERGY REQUIRED FOR ARC-HEATED HELIUM DRIVER

Although the length $l_D$ for helium drivers varies significantly with $T_4$, the arc energy required to heat the helium is rather insensitive to $T_4$. The equation for this energy is

$$E = A l_D \rho c_v (T_4 - T_i) \qquad (19)$$

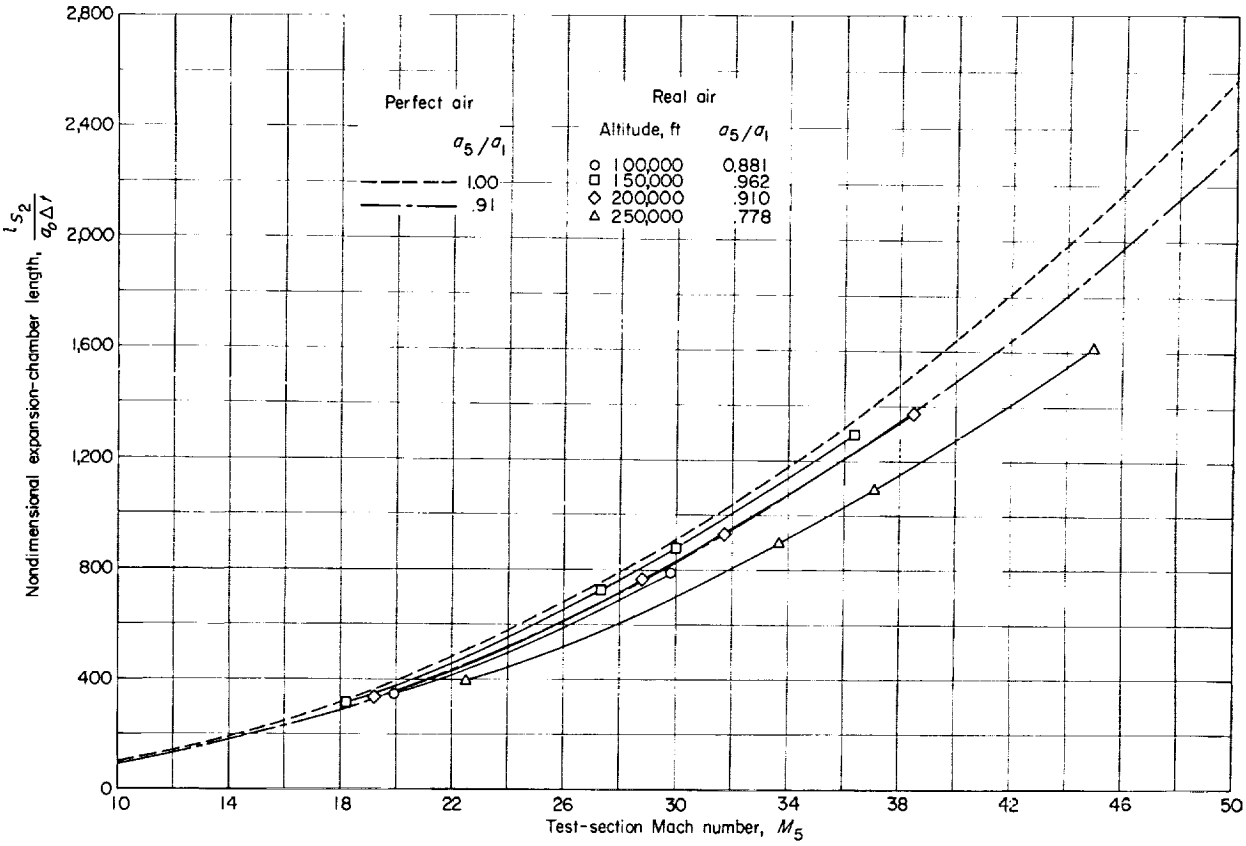


FIGURE 14.—Relation between accelerating-chamber length and test-section Mach number.

$$\frac{E}{A_4 a_0 \Delta t} = 4{,}310 \frac{l_D}{a_0 \Delta t} p_4 \left(1 - \frac{T_i}{T_4}\right) \frac{\text{joules}}{\text{ft}^3} \qquad (20)$$

where $T_i$ is the helium temperature before arc discharge, $p_4$ is measured in atmospheres, and $A_4$ is in square feet.

The curves of figure 17 illustrate this relative insensitivity of the arc-energy requirements to final temperature $T_4$. In fact, for helium, if $T_4$ is much larger than $T_i$, so that $1 - \frac{T_i}{T_4} \to 1$, the most efficient ideal driver state is that one resulting in sonic conditions downstream of the driver expansion fan (i.e., $M_3 = 1.0$).

The typical reentry trajectory from a lunar mission necessitates values of $\frac{E}{A_4 a_0 \Delta t} \approx 1.4 \times 10^6 \frac{\text{joules}}{\text{ft}^3}$, or approximately $1.5 \times 10^6$ joules per square foot of test section ($A_4 = A_1$) per millisecond of testing time.

## DISCUSSION OF MERITS AND POSSIBLE DRAWBACKS OF EXPANSION TUBE

Some of the more obvious advantages and disadvantages of the expansion tube will be discussed in this part of the report. Since this is a new device the advantages are theoretical, while the disadvantages are arrived at both theoretically and from shock-tube experience.

### MERITS

The most significant characteristic of the expansion tube is that it is the only fixed model facility known to the author which has the capability of duplicating the entire lunar-reentry velocity-altitude environment with existing state-of-the-art technology. (The technique of launching models into an opposing airflow by means of a

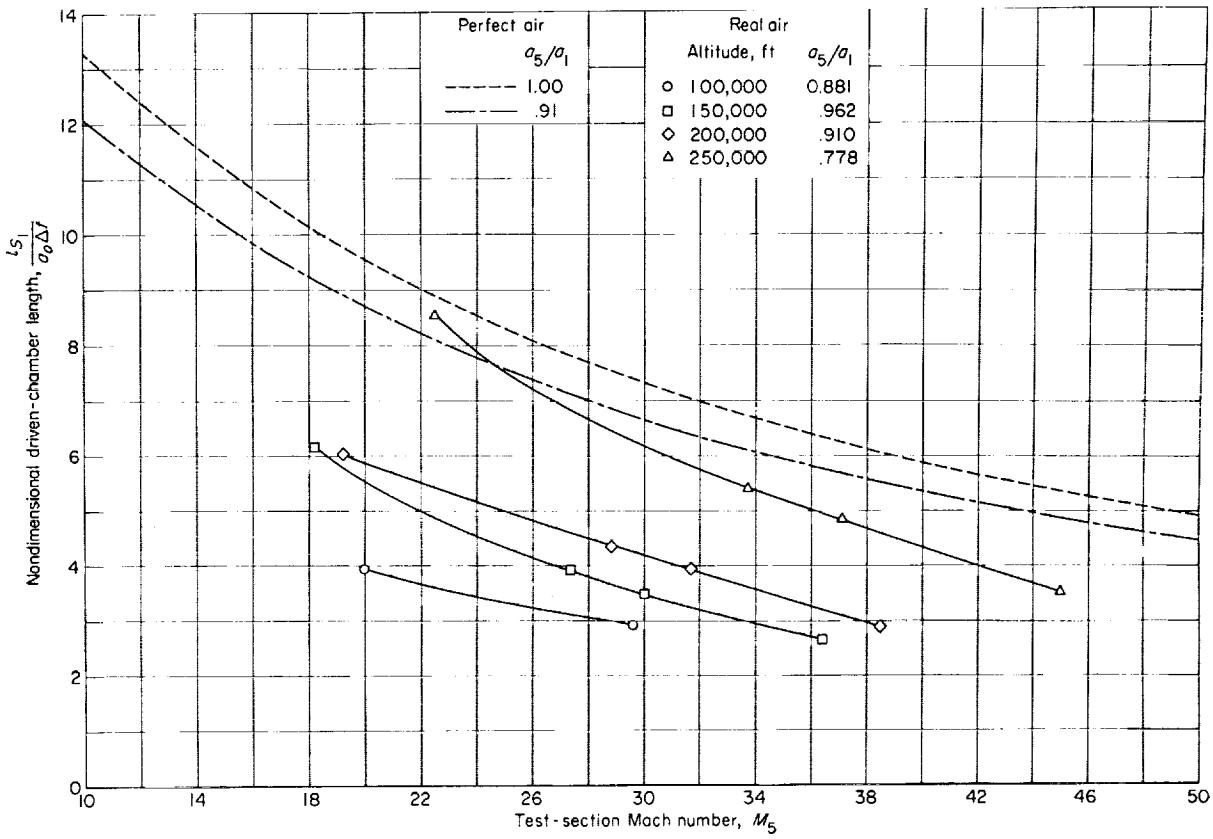


FIGURE 15.—Relation between driven-chamber length and test-section Mach number.

light-gas gun can also duplicate the lunar-reentry trajectory, but only with very small uninstrumented models.) The capability of using various test gases is an advantage common to both the shock tunnel and the expansion tube.

The superiority of the expansion tube over the conventional shock tunnel appears in the following areas:

(a) For the same driver ($p_4$, $T_4$, $\gamma_4$) and ambient test-section conditions, the velocity of the expansion tube will be more than twice that of either a reflected- or nonreflected-shock tunnel.

(b) Maximum pressures involved are several orders of magnitude less in the expansion tube than in a reflected-shock tunnel for the same lunar-reentry conditions because the expansion-tube flow does not require stagnation conditions in any part of its cycle.

(c) The test-section flow will be much nearer equilibrium in the expansion tube than in the shock tunnel. Not only is the maximum dissociation required in the cycle much less for the expansion tube, but also the expansion processes generally proceed at a slower rate so that the various energy modes have a better chance to remain in equilibrium.

(d) Variable Mach number and enthalpy are obtained without nozzles in the expansion tube. Because of real-gas effects, a shock tunnel with a fixed nozzle is unable to maintain even a constant Mach number as the altitude simulation changes (ref. 1). Thus a shock tunnel would require a set of nozzles for either testing over an altitude range at a constant Mach number or testing over a reentry trajectory at a variable Mach number. In addition, nozzle-throat erosion is no problem in the expansion tube.

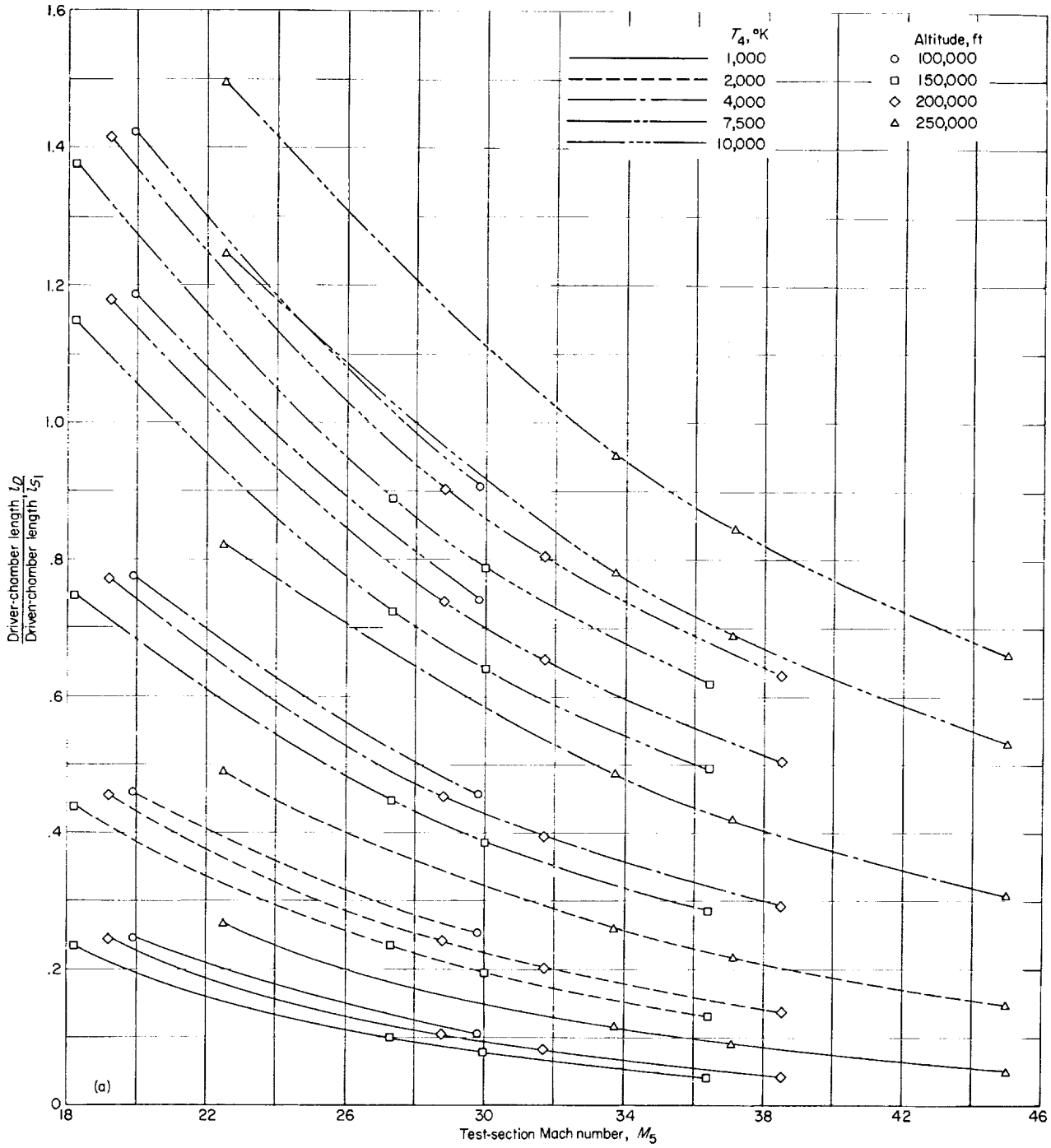


(a) Arc-heated helium drive.

FIGURE 16.—Relation between ratio of driver-chamber length to driven-chamber length and test-section Mach number

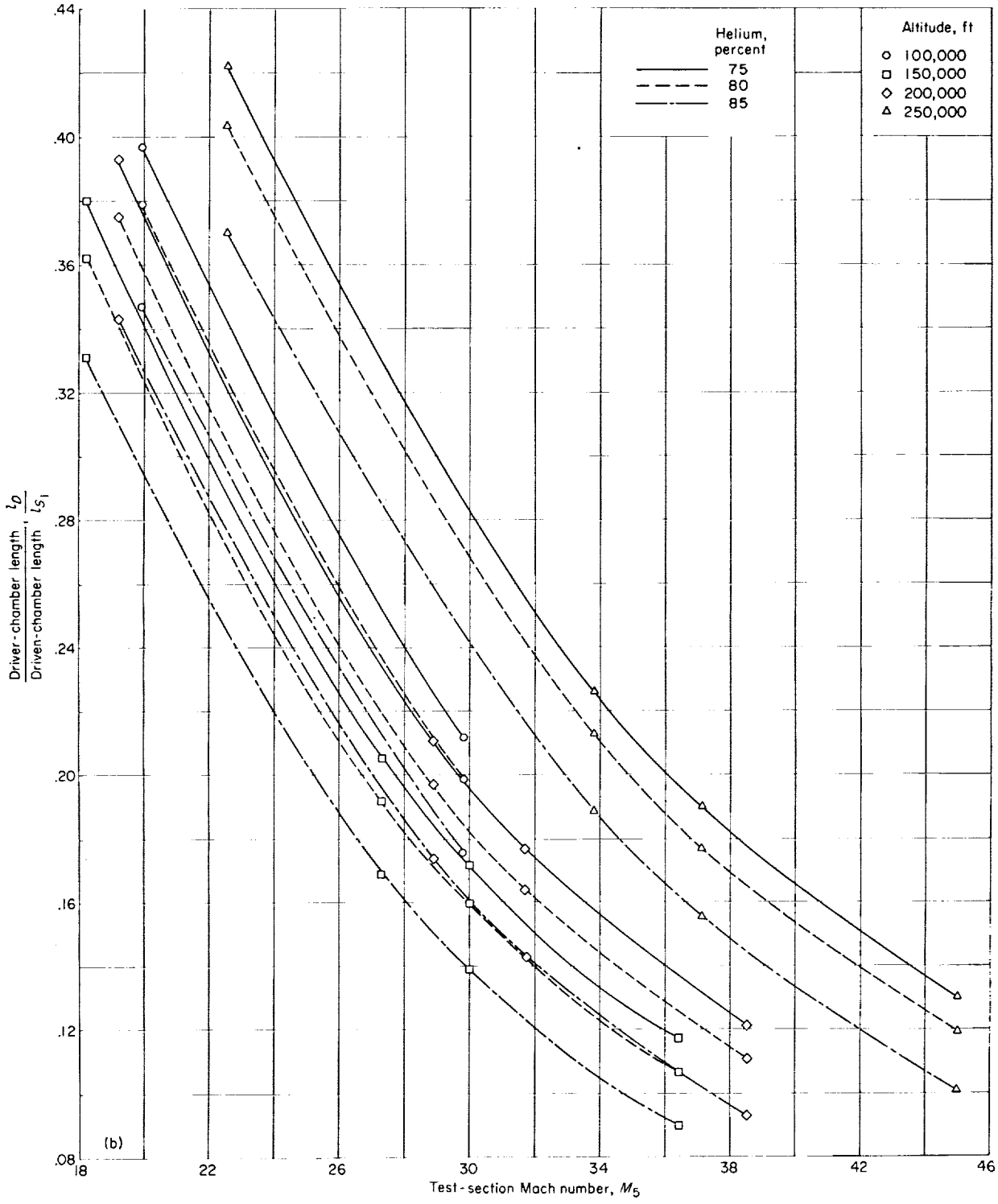


(b) Combustion drive.

FIGURE 16.—Concluded.

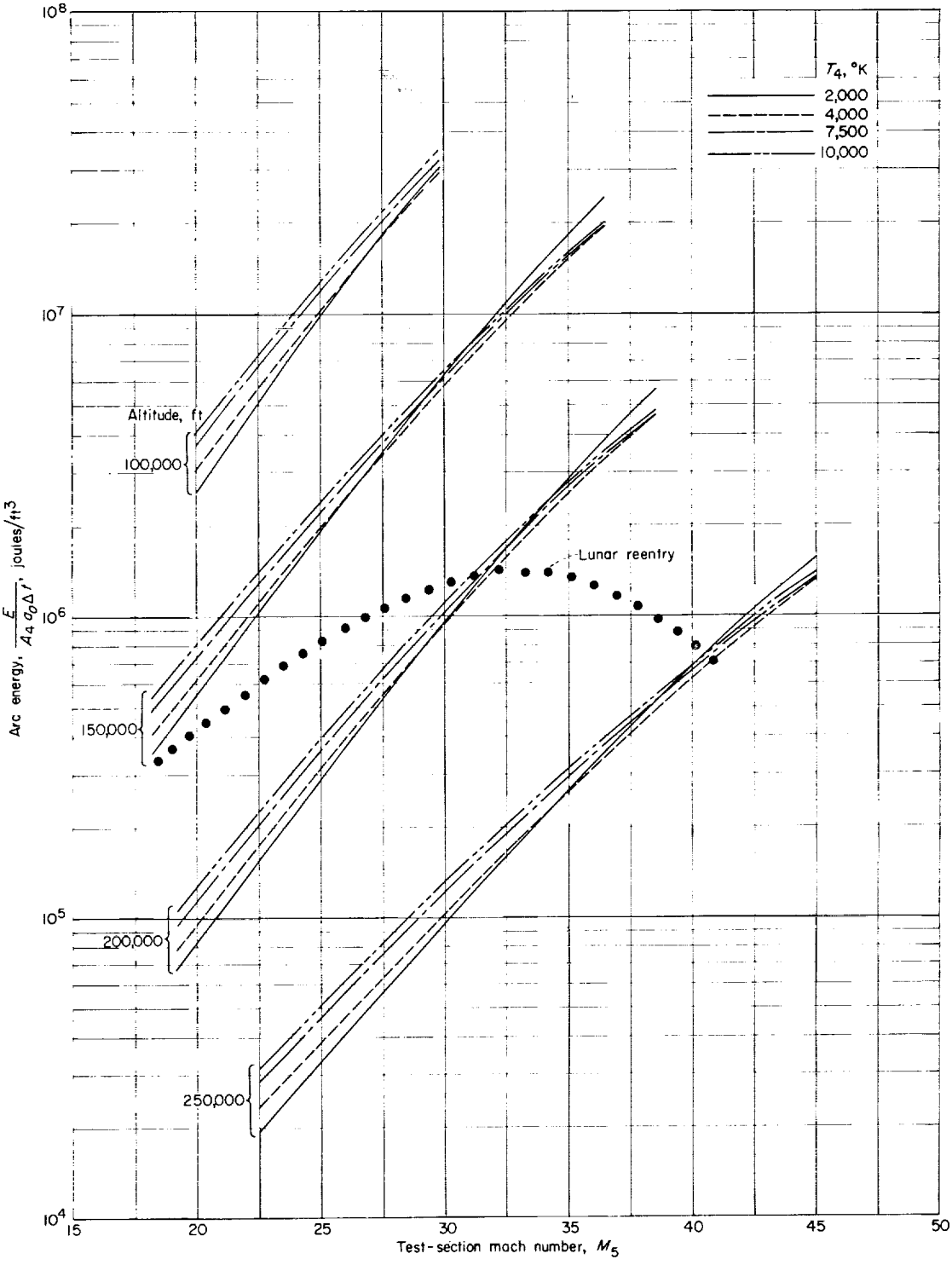


FIGURE 17.—Relation between arc energy required to heat helium driver and test-section Mach number. Helium is assumed to be a perfect gas with a temperature of 300° K before arc heating. The lunar trajectory is plotted for $T_4$=4,000° K.

### POSSIBLE DRAWBACKS

**Tube diameter.**—The main disadvantage of the expansion tube is the large diameter required of the accelerating chamber because of the long length of flow at low Reynolds numbers with resultant boundary-layer growth. No exact computations have been made of the air boundary-layer thickness, since they would require a lengthy procedure of integration through the expansion fan. (See ref. 10.) However, the order of magnitude of the thickness can be estimated from the steady-flow boundary layer existing on a flat plate of equivalent length under the same ambient conditions. If the boundary layers from opposite walls merge, the test section will no longer be a potential flow, and both total-pressure and temperature calibrations will be needed to determine whether the test results are useful. A possible modification to the basic expansion tube to shorten the length of flow required at very low Reynolds numbers involves an unsteady expansion to an intermediate pressure and a subsequent steady nozzle expansion. See sketch 1. The trade-offs

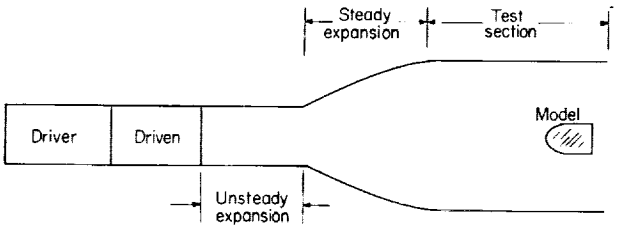


Sketch 1.

in performance, testing time, and so forth, for this modification have not yet been investigated.

**Diaphragms.**—The attainment of good diaphragm bursts appears to be one of the more difficult problems of the expansion tube. The operating pressures of the primary diaphragm are below those of many current shock tunnels, but the diameter of the driver section is much larger than the diameters of these tunnels. Consequently, a development program is required. The use of multiple diaphragms, with only part of the pressure difference applied to any diaphragm, is a possible solution. Another possibility is the sectioning of the diaphragm into many smaller areas supported by faired struts. Only the air adjacent to the secondary diaphragm is used as the test medium, and this air will be processed by the shock which will have straightened and become uniform by the time it reaches the secondary diaphragm. See sketch 2.

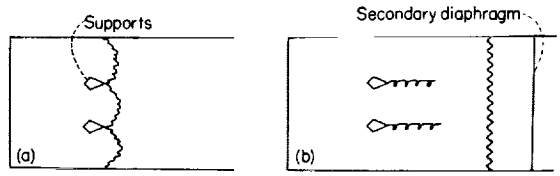


(a) Just after burst. (b) Arrival at secondary diaphragm.

Sketch 2.

The secondary-diaphragm burst must be instantaneous and ideal for the very reason that the primary-diaphragm burst may be somewhat imperfect; namely, the fact that only an extremely small part of the air originally in the driven chamber is used as the test gas. The possibility of such a rapid opening of the diaphragm may not be too remote because the secondary diaphragm is required to withstand pressures $p_1$ only of the order of a fraction of an atmosphere, whereas the imposed pressures $p_2$ available for bursting are of the order of tens of atmospheres. (See figs. 8 and 9.)

Model damage from diaphragm particles is another envisioned source of trouble. The centrifuge effect used for shock tunnels might be applied in a modified form by gradual curvature of the accelerating chamber. For experiments involving the radiation from air, the problem is reduced to that of simply isolating the part of the spectrum attributable to the diaphragm material.

**Interface mixing.**—Mixing at the interface between the test gas and the accelerating gas must also be investigated. In the shock tube attention has been focused on the forward extent of mixing, but in the expansion tube the backward extent is important.

**Shock-wave attenuation.**—Attenuation of both the primary and secondary shocks is an unknown factor. The high temperature behind the secondary shock will cause radiation from the helium which will add to the usual convective cooling and skin-friction effects that influence the attenuation,

**Turbulence.**—The extent of turbulence in the test section is another unknown. Early experiments indicated turbulent flow downstream of the expansion wave of a conventional shock tube in which there were poor diaphragm bursts that resulted in jagged edges (ref. 11). However, the expansion tube with its large diameter and a very weak secondary diaphragm may not be troubled to such a degree. The large streamwise accelerations should also tend to reduce the relative turbulence level (turbulence velocity divided by mass velocity), since the turbulence velocity perturbations will not change markedly but the mass velocity is increased in the fan. For radiation testing this turbulence may not be very important.

**Low pressure.**—The initial pressure $p_{10}$ of the accelerating gas is below the minimum required of shock tunnels. Attainment of such pressures should be no problem, since pressures of 0.1 micron may be reached without difficulty by using diffusion pumps if a little care is exercised in joint sealing and the selection of exposed surfaces to minimize outgassing.

## CONCLUDING REMARKS

The basic expansion tube considered in this paper has a theoretical potential for duplicating hypersonic flight environment far in excess of that of any other known experimental apparatus. This theoretical potential was determined for both real and perfect air by using idealized processes such as instantaneous diaphragm bursts, nonmixing entropy discontinuities, centered expansion fans, continuum flow theory, and so forth. The extent to which the actual flow will deviate from these ideal conditions is unknown, but the net effect is believed to be a decrease in performance. Modifications to the basic expansion tube (some of which are mentioned only cursorily herein) may alleviate some of the performance deficiencies. In any case, the expansion tube possesses such a high potential that further theoretical and experimental investigations are believed to be highly desirable.

LANGLEY RESEARCH CENTER,
NATIONAL AERONAUTICS AND SPACE ADMINISTRATION,
LANGLEY STATION, HAMPTON, VA., *December 5, 1961.*

# APPENDIX A

## DERIVATION OF PERFECT-GAS RELATIONS FOR SHOCK TUNNEL

### REFLECTED-SHOCK TUNNEL

The subscript 6 will be used to designate the state behind the reflected shock (i.e., the stagnation conditions for the nozzle) and the subscript 5 will denote test-section conditions. The upstream velocity of the reflected shock is $U_{s_r}$ and is treated as positive. The following equations then apply:

$$\frac{U_{s_r}}{a_1}=\sqrt{\frac{\gamma_1-1}{2\gamma_1}}\frac{2\frac{p_2}{p_1}+\frac{2}{\gamma_1-1}}{\sqrt{1+\frac{\gamma_1+1}{\gamma_1-1}\frac{p_2}{p_1}}} \tag{A1}$$

$$\approx(\gamma_1-1)\sqrt{\frac{2}{\gamma_1(\gamma_1+1)}\frac{p_2}{p_1}} \tag{A1a}$$

$$\frac{T_6}{T_{t,2}}=1+\frac{u_2^2}{c_pT_{t,2}}\frac{U_{s_r}}{u_2} \tag{A2}$$

$$\approx\frac{3\gamma_1-1}{\gamma_1+1} \tag{A2a}$$

$$\frac{T_6}{T_1}=\frac{T_{t,2}}{T_2}\frac{T_2}{T_1}\frac{T_6}{T_{t,2}}$$

$$\approx\left(1+\frac{1}{\gamma_1}\right)\left(\frac{a_2}{a_1}\right)^2\frac{3\gamma_1-1}{\gamma_1+1} \tag{A3}$$

$$\approx\frac{\gamma_1-1}{\gamma_1+1}\frac{3\gamma_1-1}{\gamma_1}\frac{p_2}{p_1} \tag{A3a}$$

$$\frac{p_6}{p_2}=\frac{\left(2+\frac{\gamma_1+1}{\gamma_1-1}\right)\frac{p_2}{p_1}-1}{\frac{p_2}{p_1}+\frac{\gamma_1+1}{\gamma_1-1}} \tag{A4}$$

$$\approx\frac{3\gamma_1-1}{\gamma_1-1} \tag{A4a}$$

Since the expansion from state ⑥ to state ⑤ is isentropic, equation (A3a) gives

$$\frac{p_2}{p_1}\approx\frac{\gamma_1+1}{\gamma_1-1}\frac{\gamma_1}{3\gamma_1-1}\left(\frac{a_6}{a_5}\right)^2\left(\frac{a_5}{a_1}\right)^2 \tag{A5}$$

$$\approx\frac{\gamma_1+1}{\gamma_1-1}\frac{\gamma_1}{3\gamma_1-1}\left(1+\frac{\gamma_1-1}{2}M_5^2\right)\left(\frac{a_5}{a_1}\right)^2 \tag{A5a}$$

$$\frac{p_1}{p_5}=\frac{p_1}{p_2}\frac{p_2}{p_6}\frac{p_5}{p_5}$$

$$\approx\frac{p_1}{p_2}\frac{p_2}{p_6}\left(1+\frac{\gamma_1-1}{2}M_5^2\right)^{\frac{\gamma_1}{\gamma_1-1}} \tag{A6}$$

$$\approx\frac{(\gamma_1-1)^2}{\gamma_1(\gamma_1+1)}\left(1+\frac{\gamma_1-1}{2}M_5^2\right)^{\frac{1}{\gamma_1-1}}\left(\frac{a_1}{a_5}\right)^2 \tag{A6a}$$

### NONREFLECTED-SHOCK TUNNEL

For isentropic steady expansion from state ② to state ⑤ the energy equation gives

$$\left(\frac{a_5}{a_2}\right)^2=\frac{1+\frac{\gamma_1-1}{2}M_2^2}{1+\frac{\gamma_1-1}{2}M_5^2} \tag{A7}$$

$$=\left(\frac{a_5}{a_1}\right)^2\left(\frac{a_1}{a_2}\right)^2 \tag{A7a}$$

$$\approx\left(\frac{a_5}{a_1}\right)^2\frac{\gamma_1+1}{\gamma_1-1}\frac{p_1}{p_2} \tag{A7b}$$

Thus,

$$\frac{p_2}{p_1}\approx\frac{\gamma_1}{\gamma_1-1}\left(1+\frac{\gamma_1-1}{2}M_5^2\right)\left(\frac{a_5}{a_1}\right)^2 \tag{A8}$$

Also,

$$\frac{p_1}{p_5}=\frac{p_1}{p_2}\frac{p_2}{p_5}$$

$$=\frac{p_1}{p_2}\left(\frac{a_2}{a_5}\right)^{\frac{2\gamma_1}{\gamma_1-1}} \tag{A9}$$

$$\approx(\gamma_1-1)\left[\frac{\gamma_1}{(\gamma_1+1)^{\gamma_1}}\left(1+\frac{\gamma_1-1}{2}M_5^2\right)\right]^{\frac{1}{\gamma_1-1}}\left(\frac{a_1}{a_5}\right)^2 \tag{A9a}$$

# APPENDIX B

## REAL-GAS SOLUTION FOR EXPANSION FAN AND SHOCK WAVE

The equation to be integrated for the expansion fan is

$$\gamma_o d\left(\frac{u}{a_o}\right)=-\left[\frac{d\left(\frac{h}{RT_o}\right)}{\frac{a}{a_o}}\right]_{s=Constant} \tag{B1}$$

Values of $\frac{a}{a_o}$ were determined from the Mollier diagram of reference 5. It was noted that a plot of $\frac{a}{a_o}$ as a function of $\frac{h}{RT_o}$ could be closely approximated by a linear function above a certain value (dependent on entropy) of $\frac{h}{RT_o}$ which was denoted as $\frac{h^*}{RT_o}$. See sketch 3.

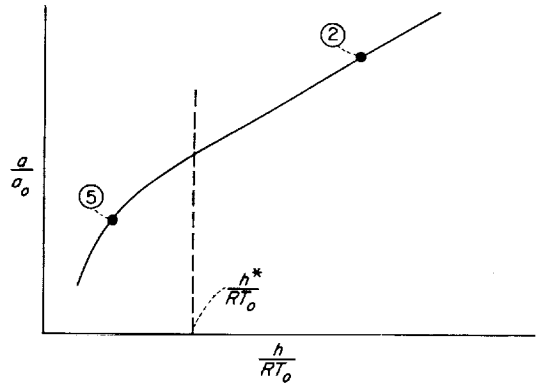


Sketch 3.

Thus for values of $\frac{h}{RT_o}>\frac{h^*}{RT_o}$, the approximation

$$\frac{a}{a_o}=B+C\frac{h}{RT_o}$$

was used, with $B$ and $C$ determined from a linear fit to the Mollier data.

Numerical integration of equation (B1) is used from $\frac{h_5}{RT_o}$ to $\frac{h^*}{RT_o}$, that is,

$$\gamma_o\left(\frac{u_5}{a_o}-\frac{u^*}{a_o}\right)=-\int_{h^*/RT_o}^{h_5/RT_o}\frac{d\left(\frac{h}{RT_o}\right)}{\frac{a}{a_o}} \tag{B2}$$

and an analytic integration is employed from $\frac{h^*}{RT_o}$ to the as yet unspecified $\frac{h_2}{RT_o}$:

$$C\gamma_o\left(\frac{u_2}{a_o}-\frac{u^*}{a_o}\right)=\log_e\frac{1+\frac{C}{B}\frac{h^*}{RT_o}}{1+\frac{C}{B}\frac{h_2}{RT_o}} \tag{B3}$$

The processes of equations (B2) and (B3) are combined to produce equation (B4):

$$C\gamma_o\frac{u_2}{a_o}+\log_e\left(1+\frac{C}{B}\frac{h_2}{RT_o}\right)=\log_e\left(1+\frac{C}{B}\frac{h^*}{RT_o}\right)+C\left[\gamma_o\frac{u_5}{a_o}-\int_{h_5/RT_o}^{h^*/RT_o}\frac{d\left(\frac{h}{RT_o}\right)}{\frac{a}{a_o}}\right] \tag{B4}$$

$$\equiv\alpha\left(\frac{u_5}{a_o},\,s_5\right) \tag{B4a}$$

The unknown state ② must be determined by finding a shock of such strength that it will generate conditions satisfying equation (B4). Consequently, consideration is now directed toward the shock wave.

An expression can be theoretically derived to relate $\frac{h_2}{RT_o}$, the enthalpy behind the shock wave, to $\frac{h_1}{RT_o}$ and $M_{s_1}$ by using the effective value of specific heat ratio $\gamma_e$ (ref. 12). This expression, equations (B5), varies less than 3 percent for $1.0\leqq\gamma_e\leqq1.4$ (which brackets all conditions for

air).

$$\frac{h_2}{RT_o}-\frac{h_1}{RT_o}=2\gamma_1\frac{T_1}{T_o}(M_{s_1}^2-1)\frac{1}{(\gamma_e+1)^2}\left(\gamma_e+\frac{1}{M_{s_1}^2}\right) \tag{B5}$$

$$\approx 2\gamma_1\frac{\gamma_e}{(\gamma_e+1)^2}\frac{T_1}{T_o}M_{s_1}^2 \qquad (M_{s_1}\gg 1) \tag{B5a}$$

When values appropriate to the charts of reference 5 $\left(\frac{h_1}{RT_o}=3.83,\ \gamma_1=1.40,\ T_1=300°\text{ K},\right.$ and $\left.T_o=273.2°\text{ K}\right)$ are used, equation (B5a) reduces to

$$\frac{h_2}{RT_o}\approx\frac{h_1}{RT_o}(1+0.20M_{s_1}^2) \tag{B6}$$

The continuity equation across the shock wave is

$$\frac{\rho_1}{\rho_2}=1-\frac{u_2}{U_{s_1}} \tag{B7}$$

The extent of the expansion fan and the strength of the shock wave are now matched by combining equations (B4), (B6), and (B7) to give

$$\frac{\rho_1}{\rho_2}\approx 1-\frac{a_o}{a_1}\frac{1}{\gamma_o C}\frac{1}{M_{s_1}}\left\{\alpha-\log_e\left[1+\frac{C}{B}\frac{h_1}{RT_o}(1+0.20M_{s_1}^2)\right]\right\} \tag{B8}$$

The desired shock strength $M_{s_1}$ and initial pressure $p_1$ are determined by plotting equation (B8) on the graph of $\frac{\rho_2}{\rho_1}$ against $M_{s_1}$ (p. 76 of ref. 5) and finding the values of $p_1$ and $M_{s_1}$ which gives $s_2=s_5$. (See sketch 4.) By such a procedure $M_{s_1}$ is rapidly evaluated because the variation of $M_{s_1}$ with $\frac{\rho_2}{\rho_1}$ in equation (B8) is small (nearly vertical line in sketch). Thus, although actually a simultaneous solution is required for $M_{s_1}$ and $p_1$, the value of $M_{s_1}$ is in essence determined independently first and then $p_1$ is evaluated.

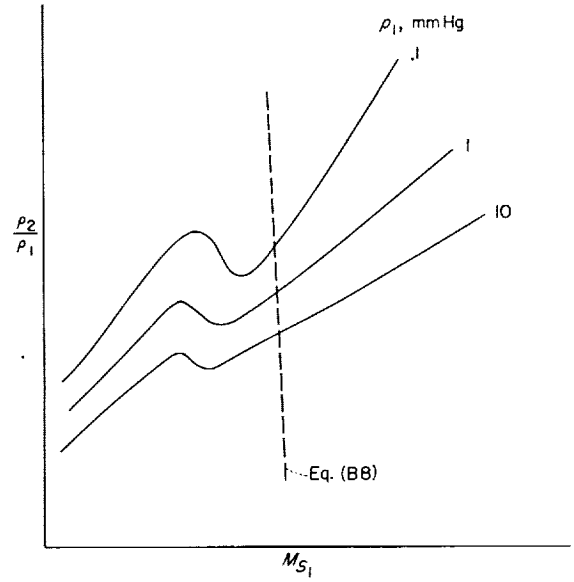


Sketch 4.

## REFERENCES


1. Hertzberg, A., Wittliff, Charles E., and Hall, J. Gordon: Summary of Shock Tunnel Development and Application to Hypersonic Research. Rep. No. AD-1052-A-12. (Contract AF 18(603)-10), Cornell Aero. Lab., Inc., July 1961.
2. Lin, Shao-Chi, and Fyfe, Walter I.: Low-Density Shock Tube for Chemical Kinetic Studies. Res. Rep. 91 (AFBMD TR 60-183), Avco-Everett Res. Lab., July 1960.
3. Page, William A., Canning, Thomas N., Craig, Roger A., and Stephenson, Jack D.: Measurements of Thermal Radiation of Air From the Stagnation Region of Blunt Bodies Traveling at Velocities Up to 31,000 Feet Per Second. NASA TM X-508, 1961.
4. Glass, I. I., and Hall, J. Gordon: Shock Tubes. Sec. 18 of Handbook of Supersonic Aerodynamics. NAVORD Rep. 1488 (Vol. 6), Bur. Naval Weapons, Dec. 1959.
5. Feldman, Saul: Hypersonic Gas Dynamic Charts for Equilibrium Air. Res. Rep. 40, AVCO Res. Lab., Jan. 1957.
6. Moeckel, W. E., and Weston, Kenneth C.: Composition and Thermodynamic Properties of Air in Chemical Equilibrium. NACA TN 4265, 1958.
7. Minzner, R. A., Champion, K. S. W., and Pond, H. L.: The ARDC Model Atmosphere, 1959. Air Force Surveys in Geophysics No. 115 (AFCRC-TR-59-267), Air Force Cambridge Res. Center, Aug. 1959.
8. Hall, J. Gordon, and Russo, Anthony L.: Studies of Chemical Nonequilibrium in Hypersonic Nozzle Flows. Rep. No. AD-1118-A-6 (Contract AF 18(603)-141), Cornell Aero. Lab., Inc., Nov. 1959.
9. Wittliff, Charles E., and Wilson, Merle R.: Shock Tube Driver Techniques and Attenuation Measurements. Rep. No. AD-1052-A-4 (Contract AF 18(603)-10), Cornell Aero. Lab., Inc., Aug. 1957.
10. Trimpi, Robert L., and Cohen, Nathaniel B.: An Integral Solution to the Flat-Plate Laminar Boundary-Layer Flow Existing Inside and After Expansion Waves and After Shock Waves Moving Into Quiescent Fluid With Particular Application to the Complete Shock-Tube Flow. NACA TN 3944, 1957.
11. Lobb, R. K.: A Study of Supersonic Flows in a Shock Tube. UTIA Rep. No. 8, Inst. of Aerophys., Univ. of Toronto, May 1950.
12. Trimpi, Robert L., and Jones, Robert A.: A Method of Solution With Tabulated Results for the Attached Oblique Shock-Wave System for Surfaces at Various Angles of Attack, Sweep, and Dihedral in an Equilibrium Real Gas Including the Atmosphere. NASA TR R-63, 1960.


U.S. GOVERNMENT PRINTING OFFICE: 1963